The body-wave magnitude m_b: an attempt to rationalize the distance-depth correction $q(\Delta, h)$

Nooshin Saloor and Emile A. Okal

Department of Earth and Planetary Sciences, Northwestern University, Evanston, IL 60208, USA. E-mail: emile@earth.northwestern.edu

SUMMARY

We explore the possible theoretical origin of the distance–depth correction $q(\Delta, h)$ introduced 75 yr ago by B. Gutenberg for the computation of the body-wave magnitude m_b, and still in use today. We synthesize a large data set of seismograms using a modern model of P-wave velocity and attenuation, and process them through the exact algorithm mandated under present-day seismological practice, to build our own version, q_{SO}, of the correction, and compare it to the original ones, q_{45} and q_{56}, proposed by B. Gutenberg and C.F. Richter. While we can reproduce some of the large scale variations in their corrections, we cannot understand their small scale details. We discuss a number of possible sources of bias in the data sets used at the time, and suggest the need for a complete revision of existing m_b catalogues.

Key words: Body waves; Computational seismology; Earthquake source observations.

1 INTRODUCTION AND BACKGROUND

Ever since Vvedenskaya (1956) and later Knopoff & Gilbert (1959) introduced the double-couple as a physical representation of a seismic source, its moment M_0 has been used as the preferred quantitative measure of earthquake sources, notably through algorithms of centroid moment tensor inversion (Dziewonski *et al.* 1981). Yet, the body-wave magnitude m_b, initially introduced by Gutenberg (1945a, b), remains to this day a valuable quantifier of the high-frequency characteristics of a seismic source. Its algorithm was formalized as one of the 'Prague formulæ' by a committee of Russian and Czech scientists following recommendations formulated at the 1960 Helsinki meeting of the International Union of Geodesy and Geophysics (Kárník *et al.* 1962; Vaněk *et al.* 1962)[1] and has remained unchanged under the recommendations of successive working groups of the International Association of Seismology and Physics of the Earth Interior [IASPEI], most recently in their 2013 Report (Anonymous 2013).

Specifically, we recall that the computation of m_b proceeds as follows:

(i) A time window following the P wave first arrival is isolated from a short-period seismogram, containing the generalized P wave (including surface reflections pP and sP).

(ii) The maximum amplitude of ground motion in that window (A, in μm) is retained.

(iii) The dominant period T of the wave train at the time of that maximum amplitude is measured (in seconds); it is recommended that this period be close to 1 s, but in no case should it exceed 3 s.

(iv) The magnitude m_b is then obtained as

$$m_b = \log_{10}\left[\frac{A}{T}\right] + q(\Delta, h), \qquad (1)$$

where $q(\Delta, h)$ is an empirical correction depending on distance Δ and focal depth h, proposed by Gutenberg & Richter (1956, fig. 5) and later reproduced by Richter (1958, fig. VIII-6, p. 688). It is shown here on Fig. 1.

The use of the ratio (A/T) in (1) expresses the goal, by the founding fathers of magnitude scales, B. Gutenberg and C.F. Richter, to associate magnitude with energy, the latter taken in its kinetic form as proportional to the square of ground velocity, hence the use of the ratio of amplitude to period. However, and as discussed in detail by Okal (2019), this relationship exists only in the case of a harmonic oscillator, whereas any seismic source generally features a broad spectrum.

The situation is made more intriguing by the fact that the correction $q(\Delta, h)$ on Fig. 1 differs significantly from its original version introduced by Gutenberg (1945b; fig. 2); and reproduced here on Fig. 2. As explained by Veith & Clawson (1972), it appears that this revision was meant to smooth excessive scatter among magnitude residuals by introducing station corrections of up to ±0.4 units of magnitude (Gutenberg 1945b, table 1; Gutenberg & Richter 1956). Such station biases are known today to occasionally reach even larger values, and are interpreted in modern terms as expressing lateral heterogeneity in receiver crustal structure and lateral attenuation, the latter documented, for example, by Der *et al.* (1985);

---

[1] This landmark report was published simultaneously in Moscow (Vaněk *et al.* 1962) and Prague (Kárník *et al.* 1962). The different listing of co-authors reflects the use of different alphabetical orders in the cyrillic and latin alphabets.
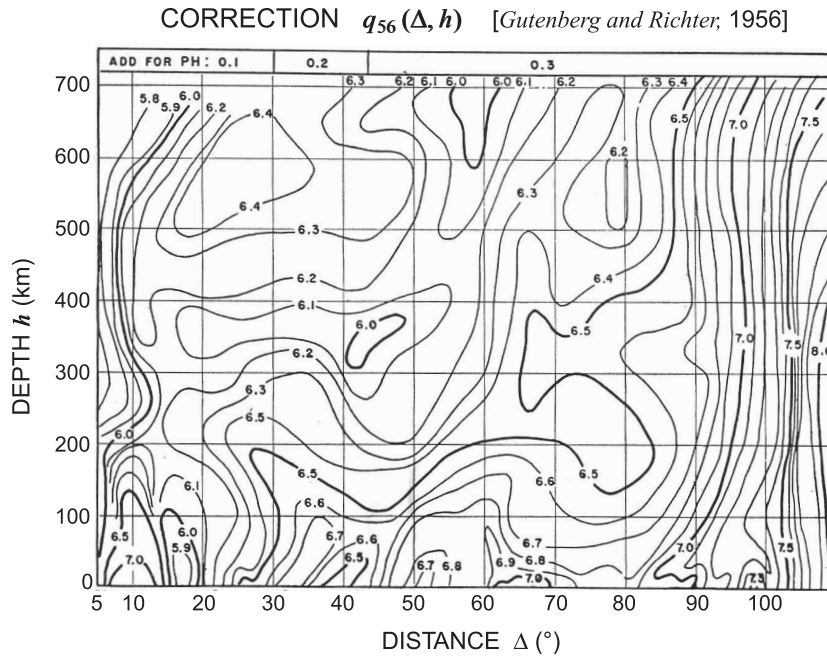
CORRECTION $q_{56}(\Delta, h)$ [*Gutenberg and Richter,* 1956]

Figure 1. 'Revised' correction $q_{56}(\Delta, h)$ mandated by the Prague Commission (Kárník *et al.* 1962), and still in use today (Anonymous 2013). Adapted from Gutenberg & Richter (1956).
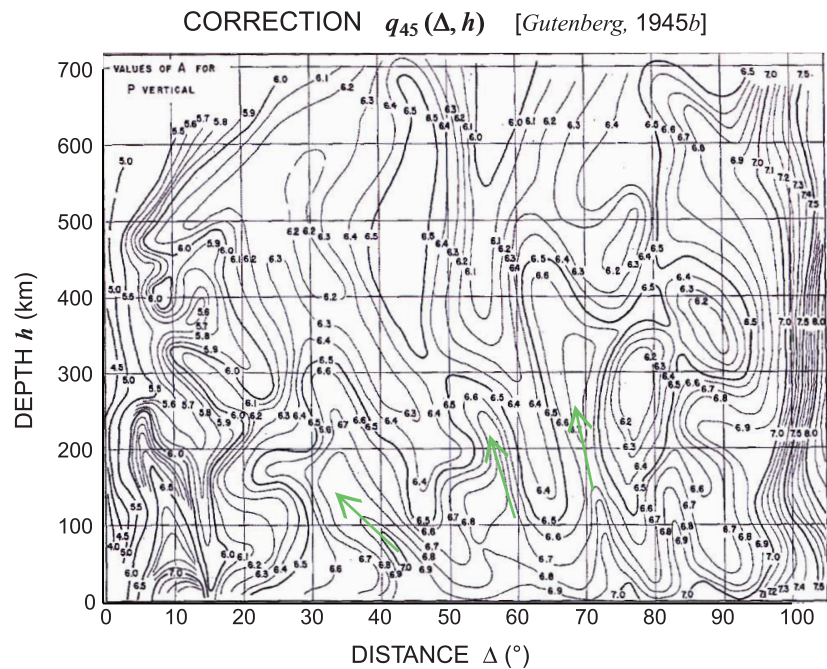

CORRECTION $q_{45}(\Delta, h)$ [*Gutenberg,* 1945b]

Figure 2. Same as Fig. 1 for the original correction $q_{45}(\Delta, h)$, adapted from Gutenberg (1945b). As discussed in the text, the green arrows indicate domains where a strong gradient of q cuts obliquely across the diagram.

however, we will show in Section 4 that such corrections may be biased by other factors.

Note further that C.F. Richter uses the notation $A(\Delta, h)$ and Gutenberg (1945b) $Q(\Delta, h)$. However, throughout this study, we shall keep the notation $q(\Delta, h)$ to avoid confusion with ground displacement (A in the majority of B. Gutenberg and C.F. Richter's relevant papers), and with the anelastic attenuation coefficient, nowadays universally referred to as Q^{-1}. We will refer to Gutenberg's

(1945b) correction factor (Fig. 2) as $q_{45}(\Delta, h)$, and to Gutenberg & Richter's (1956) more definitive version, shown on Fig. 1, as $q_{56}(\Delta, h)$.

To our knowledge, the shapes of the contours graphed on Fig. 1 have never been explained, and it is the purpose of this paper to explore their possible justification in the framework of modern theoretical seismology. We wish to emphasize here that our goal is not to propose yet another magnitude scale, but rather to research,

Table 1. Statistical comparison of the various corrections $q(\Delta, h)$.

	r_{min}	r_{max}	Average $<r> \pm \sigma$	Median r	Tenth percentile	Ninetieth percentile	Average $<|r|>$	Regression a, b	Correlation Coefficient
$r_{SO, 56}$	-0.89	0.74	0.12 ± 0.34	0.20	-0.38	0.52	0.32	$0.53, 3.12$	0.37
$r_{SO, JD}$	-0.89	0.76	0.12 ± 0.34	0.19	-0.31	0.51	0.31	$0.55, 3.01$	0.38
$r_{SO, 45}$	-1.01	0.94	0.08 ± 0.36	0.05	-0.39	0.53	0.36	$0.43, 3.75$	0.30
$r_{SO, VC}$	-0.86	1.11	0.47 ± 0.36	0.54	-0.03	0.87	0.53	$0.47, 3.71$	0.46
$r_{VC, 56}$	-1.04	0.11	-0.35 ± 0.21	-0.31	-0.66	-0.13	0.35	$1.12, -1.09$	0.79
$r_{VC, JD}$	-1.04	0.14	-0.35 ± 0.20	-0.32	-0.65	-0.14	0.35	$1.13, -1.21$	0.80
$r_{VC, 45}$	-1.00	0.27	-0.39 ± 0.23	-0.39	-0.71	-0.09	0.40	$1.01, -0.48$	0.72
$r_{56, 45}$	-0.54	0.54	-0.04 ± 0.19	-0.04	-0.28	0.20	0.15	$0.70, 1.87$	0.70
$r_{JD, 45}$	-0.52	0.53	-0.04 ± 0.19	-0.04	-0.27	0.20	0.15	$0.71, 1.86$	0.71
$r_{JD, 56}$	-0.14	0.13	0.00 ± 0.03	0.00	-0.04	0.05	0.03	$1.00, 0.03$	0.99

Note: $r_{A, B}$ is defined as $(q_A - q_B)$.

from the point of view of historical seismology, the origin of the distance–depth correction, as proposed by Gutenberg (1945b) and Gutenberg & Richter (1956).

In this context, we start (Section 2) with a detailed review of the origin of eq. (1), and of the probable method by which the various versions of the function q were obtained. Unfortunately, in addition to B. Gutenberg (1889–1960) and C.F. Richter (1900–1985), all the Prague committee members whose insight might have been invaluable in this context, since they probably examined the question in great detail, have now passed away, the last one being Dr Jiří Vaněk who died in 2018 at age 90. Thus, the only materials helping shed light on this problem are the original contributions published by B. Gutenberg and C.F. Richter.

In Section 3, we then use a large set of modern synthetic seismograms computed for various source depths and receiver distances, but for the same seismic moment, and generate our own version of the correction, $q_{SO}(\Delta, h)$. In Section 4, we compare it to q_{45} and q_{56} (Gutenberg 1945b; Gutenberg & Richter 1956), and conclude that we can reproduce some large scale features of the original q functions, but cannot explain the nature or origin of the more detailed variations introduced on a small scale in those functions by the founding fathers. In Section 5, we present a pilot test of 17 large recent earthquakes, which suggests that a bias could exist between classical m_b values for shallow and deep earthquakes of comparable moments.

2 THE DERIVATION OF EQ. (1)

In this section, we examine and paraphrase the fundamental contributions by Gutenberg & Richter (1942) and Gutenberg (1945a, b), in order to reconstruct as best as possible the steps they took to obtain eq. (1). The occasionally excruciating detail in the following paragraphs is motivated by the need to keep track of the limitations underlying many assumptions openly or tacitly made by the authors, following the approach in Okal's (2019) recent investigation of the various relations they proposed over the years between energy and magnitude.

As stated by Gutenberg (1945b), the obvious motivation behind the development of eq. (1) was to extend the concept of magnitude to earthquakes of all depths. We recall that magnitudes were originally defined by Richter (1935) for Southern California earthquakes, all of them shallow and recorded locally on torsion instruments (an algorithm which would correspond to a present-day local magnitude M_L). The concept was soon extended to teleseismic distances by Gutenberg & Richter (1936), using the dominant phases on global records, that is, surface waves with periods around 20 s.

In principle, the generation of a distance correction [pioneered by Richter (1935, table 1)] is relatively straightforward, as it is intended to yield the same magnitude for a single earthquake measured at different distances.

The situation is of course different with a depth correction, since a shallow source and a deep one must constitute two separate events. From an observational standpoint, and in the absence of an independent physical measurement of their source, there should be no obvious reason why two such earthquakes should have the same magnitude. In this context, Gutenberg & Richter (1942) and later Gutenberg (1945a, b) relied on a theoretical approach to develop a correction depending on source depth through an estimate of the seismic motion at the Earth's surface from a buried source of a given 'size', which Gutenberg (1945b) clearly intended to relate to radiated energy, stating:

"...it seems best by far to define the magnitude in such a way that two earthquakes of the same magnitude have the same energy, regardless of depth."

In this process, B. Gutenberg was attempting a connection to *"an absolute scale, in which the numbers refer* [...] *directly to shock energy* [...] *measured in physical units"* (Richter 1935). The main problem in this context is that, at such an early stage in the development of theoretical seismology, and despite valiant efforts in this respect, B. Gutenberg only had what must be regarded today as a rudimentary command of the energy radiated by a seismic source (Okal 2019), which at any rate constitutes only a fraction of the total energy transfers associated with an earthquake (Chao *et al.* 1995).

2.1 Shallow sources (Gutenberg 1945a)

In preparation for the extension of magnitudes to deep earthquakes, which do not generate significant surface waves, Gutenberg (1945a) first investigated the possibility of measuring magnitudes of shallow earthquakes on shorter-period body waves, including the phases *P*, *PP* and *S*. In this work, we consider only *P*, since short-period magnitudes are no longer measured from *PP* or *S* phases, which suffer considerable anelastic attenuation. We note, however, that a detailed reading of Gutenberg (1945a) fails to ascertain precisely the period (or more probably the range of periods) used by the author: a mention is made on p. 60 of 'waves having a period of a very few seconds', and specifically of a period of 0.5 s on p. 62, albeit in the context of local shocks. From his statement on p. 58 regarding the Benioff short-period seismometer (Benioff 1932), and based on our experience with such records, it can be assumed that at least a subset of Gutenberg's (1945a) measurements were performed around $T = 1$ s.

The approach taken by Gutenberg (1945a, b) for the calculation of body-wave magnitudes uses the theoretical model of a point source buried at a depth h and of geometrical optics, to estimate the seismic energy flux at a distance Δ which can be teleseismic or regional. In the first paper, Gutenberg (1945a, table 4) derives distance corrections for body-wave magnitudes of shallow earthquakes, based on the now classical expression of geometrical spreading (which he had helped formulate as L. Geiger's co-author of Zöppritz *et al.* (1912), written up following Karl Zöppritz' untimely death in 1908). The author first relates epicentral ground displacement to the energy E_1 in a 'single body wave', meaning a single oscillation of period T. Proceeding to simply add the energies of such oscillations, B. Gutenberg then makes the assumption that the 'duration' of the wave train at the epicenter, t_0, grows with magnitude like the dominant period T_0 at the epicentre, in other words that the number of oscillations in the P wave at the epicenter is independent of magnitude, which in turn means that the total energy E radiated at the source should be proportional to E_1, or to the quantity $(A/T)^2$ measured on a single oscillation. Gutenberg (1945a) then combines this result with the empirical formula between energy and magnitude proposed by Gutenberg & Richter (1942; eq. 35)

$$\log_{10} E = 11.3 + 1.8\,M \qquad (2)$$

(E in ergs) to suggest that the quantity

$$0.9\,M - \log_{10} \frac{A}{T} + \log_{10} W, \qquad (3)$$

where W is the geometrical spreading factor, should have a 'nearly constant value for all [...] P waves' (note that Gutenberg (1945a) uses the notation w for the vertical ground displacement A). He then substitutes the factor 0.9 with the rounded value 1, reaching the expression

$$M = \log_{10} \frac{A}{T} + q\,(\Delta) + 0.1\,(M - 7), \qquad (4)$$

where the distance correction $q\,(\Delta)$ is just $(-\log_{10} W)$ plus the constant 0.7. Noting further that

"As most shocks [studied] *at distant stations have magnitudes between 6 and 8, the absolute value of* $0.1\,(M - 7)$ *rarely exceeds 0.1"*,

Gutenberg (1945a) simply discards the relevant correction in the last term of (4), which then takes the form (1) with fixed h, in which he proposes to compute the function $q\,(\Delta)$ theoretically as resulting from geometrical spreading.

We note here that the 'geometrical spreading' function used by Gutenberg (1945a) contains an 'absorption factor' that we would relate in modern terms to anelastic attenuation, and which he represents in the form of an energy decay

$$a = \exp\,(-k\,D), \qquad (5)$$

where D is the 'whole path' of the waves, and the constant k is taken as 1.2×10^{-4} km^{-1}.

Before proceeding to the case of deep sources, it is worth examining critically some of the assumptions underlying the above algorithm. Okal (2019) has pointed out that the slope 1.8 in (2), a crucial element of the above derivation, was obtained empirically by the authors from the variations with magnitude of epicentral ground acceleration and signal duration, both of which are unsustained by modern seismological theory. Note also that the value 1.8 in (2) was replaced with 1.6 in Gutenberg & Richter (1954) and later 1.5 in Gutenberg & Richter (1956). Such lower values would tend to

increase the correction term to the right of (4), and to make it less justifiable to simply discard it to obtain (1).

In addition, the proposed linear growth between source duration t_0 and dominant period T_0 is also questionable. As discussed by Okal (2019), modern theory could indeed suggest that both would grow like $M_0^{1/3}$ since the former would be controlled by the duration of rupture, and hence fault length, while the latter could be related to rise time, through the inverse of a source corner frequency. However, this simple argument will break down for a large earthquake, especially since the waves actually recorded on a seismogram are filtered by anelastic attenuation and instrument response.

Finally, the handling of anelastic attenuation in the form of (5) is highly questionable, since modern studies describe its effect on energy through a factor

$$a' = \exp\,(-\omega t / Q), \qquad (6)$$

where Q is the so-called quality factor of the wave [unrelated to the correction q in (1)]. In particular, for the energy of P waves generated by shallow shocks, a first-order approximation to the effect of attenuation is often taken as $\exp\,(-\omega t^*)$ with $t^* = 1$ s (Carpenter 1965), which can be explained by the concentration of anelastic attenuation during the wave's transits through the asthenosphere, largely independent of distance Δ. The expressions a and a' could be reconciled, for example, for a 'whole path' D of the length of the Earth's radius, typical of a teleseismic layout, only by assuming a period $T = 2\pi\,t^* / kD = 8$ s, much longer than the realm of short-period body waves, mandated to remain under 3 s under modern practice (Anonymous 2013). Note incidentally that Gutenberg (1945a) proposes to apply (5) to both P and S waves with the same value of k, and ends his paper with the conclusions that absorption is similar in the mantle and the core, and that radiated energy is partitioned equally at the source between P and S waves, all statements irrevocably negated under modern seismological theory.

2.2 Deep sources (Gutenberg 1945b)

Turning now to the case of deeper sources, Gutenberg (1945b) provides only very scant information on the procedures which he must have used to achieve the degree of complexity of Fig. 2. He assumes that the same relationship (2) applies between energy and magnitude regardless of depth, and that ground displacement could be similarly related to radiated energy through geometrical spreading. No mention is made of the handling of 'absorption' (anelastic attenuation), but it can be assumed from the universal character which Gutenberg (1945a) gives eq. (5) that it was also used, with the same value of k, for deep sources.

Gutenberg (1945b; p. 118, 4th paragraph) then computed theoretically the resulting values of $q\,(\Delta, h)$ (that he calls A) at 200, 400 and 600 km, and interpolated the results at other depths. Note at this stage that there is no way to obtain the level of complexity of $q_{45}\,(h)$ (at fixed Δ) evidenced on Fig. 2, for example, at $\Delta = 25°$, 65° or 85°, from an interpolation between just four values of depth [including the shallow one from Gutenberg (1945a)].

We note also that the earthquake depths used by Gutenberg (1945b) were obviously marred by imprecision and inaccuracy. In this context, we examined 133 intermediate and deep events listed in *Seismicity of the Earth* (Gutenberg & Richter 1954) and successfully relocated with a floating depth into the ISC-GEM catalogue (Bondár *et al.* 2015). We found that the relocated depths differed anywhere from 0.1 to 149.7 km from the historical ones, the average being 16 km and the root mean square 20 km. These numbers

mean that it was illusory in those days to envision a precision (let alone an accuracy) on hypocentral depths greater than 15–20 km, and therefore to design a function q featuring significant variations (at fixed Δ) over depth intervals of that range or smaller.

In the same paragraph, B. Gutenberg later states that additional corrections were made by considering, for shallow sources and as a function of distance Δ, individual residuals observed between actual measurements and theoretical ones predicted from geometrical spreading. Such 'shallow' corrections were then included in the final $q_{45}(\Delta, h)$ for deeper sources, under the assumption that they could be equally applied, as long as the ray parameter (p in modern theory) remained constant, which he mentioned, implied only a slight reduction in distance with increasing source depth. This remark could conceivably explain the bending of some of the resulting contours (see green arrows on Fig. 2); however the slopes of this bending (about $-16°$ over 200 km around $\Delta = 40°$, $-8°$ over 200 km at $60°$ and $-10°$ over 400 km at $70°$) would lead to take-off angles at the source of $83°$, $76°$ and $68°$, respectively, which are totally unrealistic at those distances. This leaves the origin of the complex contours on Fig. 2 suspect.

2.3 Later investigations

In the late 1960s, and following investigations of the anelastic attenuation inside the Earth (e.g. Anderson *et al.* 1965), the inadequacy of modelling absorption through eq. (5) had became evident, as well as the presence of lateral heterogeneity in attenuation at short distances and for shallow sources, notably in the recordings of underground explosions (Evernden 1967).

Veith & Clawson (1972) later used a data set of records from large explosions (both conventional and nuclear and located both underground and in the oceanic water column), as well as from a number of well-located earthquakes, all at distances ranging from $0°$ to $100°$, to separate true geometrical spreading from the effect of anelastic attenuation, modeled using the more realistic form (6). They then inverted their observations into a model (which they call $\widehat{Q}$) of the intrinsic quality factor Q_α of P waves as a function of depth in the mantle, following a technique of incremental depth penetration reminiscent of the classic Herglotz–Wiechert inversion. Combining it back with a model of geometrical spreading derived from a profile of P-wave velocities in the mantle, they obtained a new distance-depth correction for body-wave magnitudes (which they call a 'P' factor), shown in Fig. 3, which is clearly much smoother than either Gutenberg's (1945b) q_{45} or Gutenberg & Richter's (1956) q_{56}. Note that Veith & Clawson (1972) use measurements of peak-to-peak amplitudes, whereas B. Gutenberg and C.F. Richter's are made in the lineage of Richter's (1935) zero-to-peak measurements; furthermore, Veith & Clawson (1972) express their amplitude-to-period ratios in nanometers per second. Thus, in order to compare them to q_{45} or q_{56}, a constant of 3.3 must be added to their P factors. We will refer to the resulting values as corrections $q_{VC}(\Delta, h)$.

Veith & Clawson's (1972) $\widehat{Q}$ model (shown on their Fig. 4) features prominent attenuation in the asthenosphere, between depths of 80 and 300 km, and is more in line with our present understanding of the Earth's structure (Romanowicz & Mitchell 2015) than predecessors such as Anderson *et al.*'s (1965) MM8 model, which generally features too little attenuation under today's understanding, or Teng's (1968) Model G, which has too much. However, $\widehat{Q}$ obviously trades off with details of the velocity structure used, and in this respect, it is unfortunate that it was built using Herrin's (1968)

velocity profile, which features neither a prominent low-velocity zone in the asthenosphere, nor the mantle discontinuities delimiting the transition zone, around 410 and 660 km (Johnson 1967; Julian & Anderson 1968). The latter induce classical triplications leading to caustics and strong variations in amplitude at distances less than $30°$ (Johnson 1967; Burdick & Helmberger 1978; Ebeling & Okal 2012).

Finally, we note that the data file annexed to Anonymous (2013) as a digitized version of $q_{56}(\Delta, h)$ and used under operational procedures at agencies such the United States Geological Survey's National Earthquake Information Center (NEIC) and the International Seismological Center (ISC) (J. Dewey and D. Di Giacomo, pers. comm., 2019), is significantly smoothed with respect to the original published by Gutenberg & Richter (1956), as a result both of a coarse sampling in depth, and of rounding values to 1/10 of a logarithmic unit. We will refer to the digital version of that correction as $q_{JD}(\Delta, h)$.

2.4 Shortcomings of the Prague $q(\Delta, h)$

In summary, the function $q_{56}(\Delta, h)$ proposed by Gutenberg & Richter (1956) and enshrined by the Prague committee (Kárník *et al.* 1962) suffers from the following shortcomings (as well as its predecessor q_{45} (Gutenberg 1945b)):

(1) It features too much complexity to be realistically derived from our present knowledge (and *a fortiori* that of the founding fathers) of the Earth's interior.

(2) It is based on a direct relationship between $(A/T)^2$ and energy, which holds only for monochromatic wave trains.

(3) It uses eq. (2), itself based, at least tacitly, on perceived scaling laws which are not upheld by present-day observations (Okal, 2019, e.g. p. 3842).

(4) It uses an unrealistic formulation of anelastic attenuation.

(5) It was derived before the existence of structure in the Earth's mantle was documented (transition zone discontinuities) or confirmed (low-velocity zone).

In addition, a large number of studies have shown over the years that the computation of m_b under a simple protocol (e.g. Anonymous 2013) leads to significant residuals among stations. In this respect, the important role of the shallowest soil layers was already noted by Milne (1898) and quantified in Southern California by Gutenberg (1957), the concept of a site response function was described by Borcherdt (1970), and the effect of receiver topography discussed by Bouchon (1973). Finally, lateral heterogeneity in attenuation was recognized as an important cause of bias (e.g. Der *et al.* 1985). As a consequence, even network m_b values can be affected by the exact station (or set of stations) selected from within the network to make the actual measurement. All these effects played a crucial role in the context of monitoring the Partial and later Comprehensive Nuclear-Test Ban Treaties, as described, for example, by North (1977) and Marshall *et al.* (1979), and reviewed extensively by Ringdal (1986) and more recently Peacock *et al.* (2017).

In this context, the form chosen for the correction q by Gutenberg (1945b), and later enshrined into the Prague formula and the present protocol, namely a function of only Δ and h, is clearly an oversimplification. Any attempt to build a more successful body-wave magnitude scale would have to take into account lateral heterogeneity in the elastic and anelastic structure of the Earth. Undoubtedly, it would perform better, that is, it would reduce or eliminate magnitude biases, since conceptually, it would use a larger parameter space, of
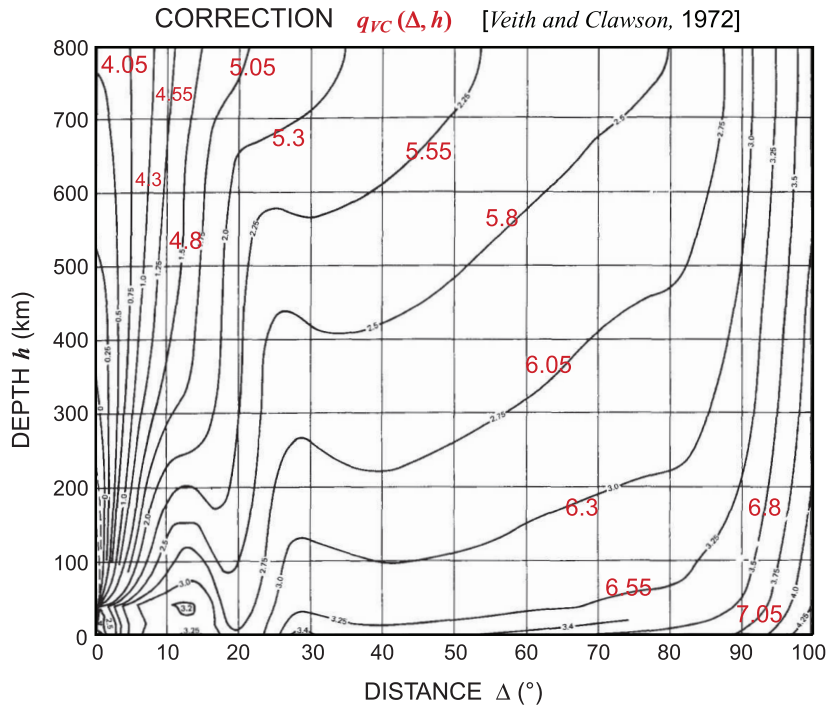
Figure 3. Correction q_{VC}, proposed by Veith & Clawson (1972) (adapted from their Fig. 9). The small numbers relate to their parameter P (amplitude measured peak-to-peak in nm). The superimposed red numbers, obtained by adding a constant of 3.3, relate to the correction q_{VC}.
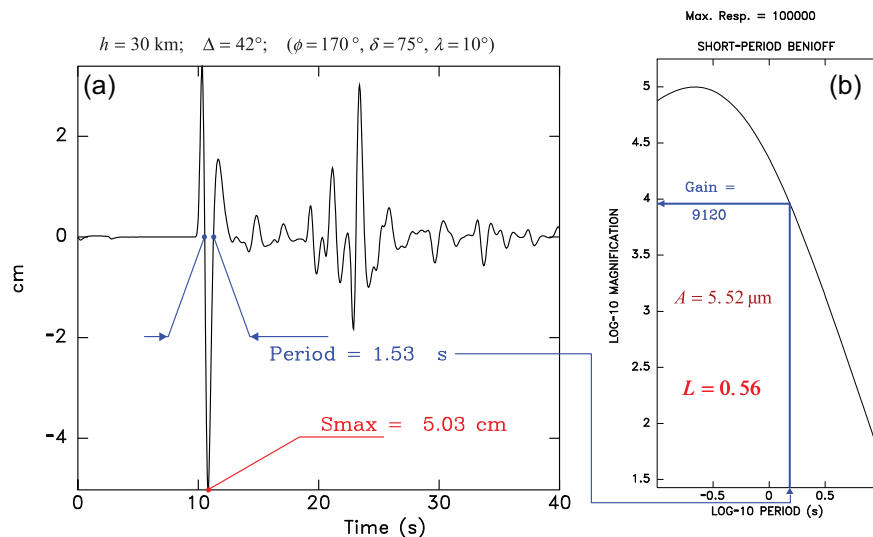

Figure 4. Sketch of the measurement of $L = \log_{10}(A/T)$ on a synthetic seismogram. The maximum absolute amplitude S_{max} (in this case 5.03 cm) is measured on the synthetic time series (a), and the period $T = 1.53$ s of that oscillation retained and transferred to the response curve of the instrument (b), from which the gain $G = 9120$ is computed. The ratio $A = S_{max}/G$ amounts to 5.52 μm from which $L = 0.56$ is inferred.

which (Δ, h) constitutes a mere subset. However, we stress once again that such is not the goal of the present study, which only aims at gaining some understanding of the origin of the complexity in q_{56} and q_{45}, restricted to being functions of only two variables.

In the next section, we compute a large number of synthetic seismograms, using a common seismic moment. In an ideal model deprived of ancillary effects such as lateral heterogeneity and local site receiver effects, an appropriate m_b algorithm should then yield the same magnitude, independent of distance and depth (notwithstanding the effect of focal geometry, which can be expected to be smoothed out by averaging over numerous receivers). As described

below, we then process this synthetic data set through the Prague-mandated algorithm for m_b, and thus build our own version of the correction, $q_{SO}(\Delta, h)$.

3 COMPUTATIONAL APPROACH

3.1 Model and parameters

Our synthetic seismograms are built using Herrmann's (2013) 'hudson96' code which utilizes a layer matrix method (Carpenter 1966; Hudson 1969), itself based on Haskell propagators (Haskell 1962).

The seismic moment is fixed at $M_0 = 10^{25}$ dyn.cm (10^{18} N.m). The Earth model used here is *ak135* (Kennett *et al.* 1995), which includes the mantle discontinuities at 410 and 660 km, with an attenuation model (Montagner & Kennett 1996) featuring a low $Q_\alpha \approx 120$ in the asthenosphere. Note that this model, which features a maximum value of Q_α around 700 km, followed by a decrease in the lowermost mantle, differs substantially from Veith & Clawson's (1972) $\widehat{Q}$. This increase of attenuation in the deep mantle, already proposed by Okal & Jo (1990), will have significant implications for the correction $q_{SO}(\Delta, h)$.

Our procedure forces a constant relationship, independent of depth, between magnitude m_b and moment M_0. This could be a departure from Gutenberg's (1945b) approach, in which he was seeking to impose a constant one between magnitude and energy E, at the time the only quantity considered as a possible physical quantifier of seismic sources. Our choice is certainly subjective, and could be regarded as inappropriate, since the 1–s m_b, characteristic of felt and destructive effects, is inherently high-frequency and more closely related to E than to M_0, a static or low-frequency concept. Indeed, as discussed in detail by Okal (2019), it is illusory to describe the size of a seismic event by a single number, as clearly evidenced by the numerous studies of variations in E/M_0 (Choy & Boatwright 1995; Newman & Okal 1998; Choy *et al.* 2006). However, recent studies have shown that the ratio E/M_0, directly related to strain release, has a relatively contained variation with depth, of about 0.4 logarithmic units (Saloor & Okal 2018), or perhaps even untraceable (Vallée 2013; Poli & Prieto 2016) . Differences in E/M_0 are then mostly attributable to local conditions derived in particular from lateral heterogeneity. In the context of our purpose in the present study, namely to research the origin of the function $q(\Delta, h)$ in the model of a laterally homogeneous Earth, it is then legitimate to associate a constant magnitude to a constant seismic moment. Finally, we note that all synthetic seismograms are obtained by solving the equations of mechanics, forced by a system of forces, that is, a moment tensor in the case of earthquakes, and are therefore expressed as a function of M_0.

3.2 The instrument

In order to reproduce the observational conditions under which magnitudes are measured, we include in our synthetics an instrumental response. This can be a complex issue, since different instruments were used over the years, from torsion systems (Richter 1935) to broadband seismometers, now the standard equipment at modern seismological stations. As our goal here is to explore the origin of B. Gutenberg's functions q_{45} and q_{56}, we elect to use the Pasadena Benioff short-period instrument (Benioff 1932) on which most of his personal readings were probably made, as suggested in Gutenberg (1945a, p. 58). The Benioff short-period seismometer is a classical electromagnetic system, featuring a pendulum period $T_p = 1$ s, a galvanometer period $T_g = 0.23$ s, weak coupling ($\mu^2 = 0.05$), and critical damping. It was to become the prototype of the short-period instrument later used in the WWSSN, albeit with a longer $T_g = 0.8$ s (Peterson & Hutt 2014). Of course, (Gutenberg 1945a, b) also relied on readings mailed to him from other observatories, since not all combinations of distance and depth were observable at Pasadena, and those records were taken on other types of instruments, for which the maximum amplitude could have been obtained at a different period; this point will be examined more in detail in Section 4.4.

3.3 The sources

In order to minimize saturation effects due to source finiteness, we use a point source and a moment-rate function in the form of a parabola with a width of only 0.2 s (Herrmann 2013). Our synthetics are thus built in violation of standard seismic scaling laws, but in conditions where the magnitude m_b should be directly proportional to $\log_{10} M_0$ (Geller 1976). We refer to Okal (2019; eq. 20a) for an updated version of that relationship, under which the common seismic moment used in our synthetics, $M_0 = 10^{25}$ dyn.cm (10^{18} N.m), should correspond to a magnitude $m_b = 6.82$.

For a given combination of source depth h and receiver distance Δ, our approach consists of generating synthetics for a large number of focal geometries and station azimuths, and of averaging the resulting logarithmic measurements. We loop over 10 values of the dip angle δ from 45° to 90°, 18 values of the slip angle λ from 0° to 170°, and 36 values, from 0° to 350°, of $\phi = \phi_f - \phi_s$, defined as the difference between the azimuths of the fault strike and of the great circle from source to receiver (in practice, we vary the fault strike, and fix the station azimuth, $\phi_s = 0°$). This amounts to a grand total of 6480 source–receiver geometries, which averages the influence of focal geometry on the recorded amplitude of the generalized *P* wave. Note that we do not need to consider events with a normal faulting component ($-180° \leq \lambda < 0°$) since they correspond to the exact opposite slip of thrust events, and their records can be obtained by simply flipping the sign of the synthetics. Nor do we need to consider dip angles less than 45°, since a double-couple always has at least one fault plane dipping 45° or more.

We then loop over source depth in 10-km increments from $h = 10$ to 690 km, and over receiver distance Δ in 1° increments from 10° to 95° for a grand total of 38 452 320 synthetic seismograms.

3.4 The magnitude measurement

Once the synthetics are created, the algorithm for the measurement of m_b follows the practice mandated by the Prague formula and the recent IASPEI working group (Anonymous 2013). An example of the computation of amplitude A and period T is detailed on Fig. 4. First, the amplitude of the recorded seismogram, S_{max}, is simply obtained as the maximum absolute value of the trace of the seismogram in the time window considered. The period T (in s) is obtained by doubling the interval separating the first zero-crossings of the time series on either side of that maximum. The ground motion A is then computed by dividing S_{max} by the gain G of the instrument at the period T, and the result expressed in microns (μm). The logarithm

$$L = \log_{10} \frac{A}{T} \tag{7}$$

is then computed, and its average taken over all source–receiver geometries, at constant distance and depth:

$$< L > (\Delta, h) = \frac{\sum\limits_{i=1}^{180} w_i \sum\limits_{j=1}^{36} \log_{10}\left[\frac{A}{T}\right]_{i,j}}{36 \sum\limits_{i=1}^{180} w_i} \tag{8}$$

In (8), j is the index varying the fault strike ϕ_f (in increments of 10° and for $\phi_s = 0°$), and i a double index combining dip and slip angles. We recall that, in order to minimize the number of synthetics computed, we consider only dips $\delta \geq 45°$. Of the resulting 180

different focal mechanisms, 108 (trending towards a strike-slip geometry) feature an auxiliary plane dipping more than 45°, and thus are sampled twice by our algorithm (once per fault plane), while the remaining 72 (approaching a thrust mechanism) are sampled only once. For that reason, we introduce in (8) a weighting factor, $w_i = 0.5$ for the former type and $w_i = 1$ for the latter. The two groups are easily separated by considering the discriminant

$$\tan^2 \lambda + \frac{1}{\cos 2\delta} \qquad (\delta > 45°) \qquad (9)$$

which is negative in the former case, positive in the latter. The denominator in (8) then takes the value $36 \times 126 = 4536$, which is the estimate of the number of independent combinations of focal mechanism and fault strike.

Since all synthetics were computed for a moment $M_0 = 10^{25}$ dyn.cm (10^{18} N.m), which should correspond to a magnitude $m_b = 6.82$ (Okal 2019), the correction $q_{SO}(\Delta, h)$ is then simply

$$q_{SO}(\Delta, h) = 6.82 - <L>(\Delta, h) \qquad (10)$$

4 RESULTS

4.1 General trends

The function q_{SO} is shown on Fig. 5. The labels refer to a number of trends, immediately evident in its distribution in the (Δ, h) plane.

(A) A broad arc featuring strong gradients of q_{SO} is identified at distances shorter than 30°. It illustrates the triplications characteristic of waves bottoming at the mantle discontinuities located at 410 and 660 km, respectively. As expected, the relevant distances decrease with increasing h, and the arc faints and eventually disappears at the short distances reached by a ray taking off horizontally at each mantle discontinuity.

This feature is obviously absent from q_{45}, q_{56} and q_{VC} which do not include the mantle discontinuities.

(B) At shorter distances and shallow depths, the bottom left-hand corner of Fig. 5 features an extremely rapid variation of q_{SO}. Similar, but not immediately comparable, trends are found in q_{VC}, q_{45}, and to a lesser extent q_{56}.

(C) At much greater depths ($h > 550$ km), and in the distance range 15–30°, we observe a zone of systematically low values of q_{SO}, which illustrate high amplitudes for rays not penetrating the deep mantle, and thus bottoming in the mantle layers featuring the highest Q_α values. This interpretation is verified by the fact that this zone is largely absent from Veith & Clawson's (1972) q_{VC}, which has a homogeneous (and high) $\widehat{Q}$ in all of the lower mantle, from 800 km down.

In consideration of the above trends (**A, B, C**), we will restrict our further comparison of the various corrections q to distances $\Delta \geq 20°$. Indeed, we note that this limitation corresponds *de facto* to that of the table of rounded q_{JD} corrections proposed by the IASPEI working group (Anonymous 2013).

(D) At larger distances, the downwards transition of the source across the mantle discontinuities is marked by an increase in q_{SO} on the order of 0.05 logarithmic unit. As discussed, for example, by Okal (1992), the amplitude of a teleseismic P wave is controlled, irrespective of its radiation pattern R^P and of anelastic attenuation, by the product of the moment tensor excitation and of the geometrical spreading factor:

$$\frac{M_0}{4\pi \rho \alpha^3} \cdot \left[\frac{\rho_h \alpha_h}{\rho_0 \alpha_0} \frac{\sin i_h}{\sin \Delta} \frac{1}{\cos i_0} \left| \frac{di_h}{d\Delta} \right| \right]^{1/2}, \qquad (11)$$

where subscripts h and 0 refer to source depth and Earth surface, respectively. Given $\sin i_h = \dfrac{\alpha_h}{r_h} \cdot \dfrac{dT}{d\Delta}$, one derives

$$\sin i_h \cdot \frac{d i_h}{d\Delta} = \frac{\alpha_h}{r_h} \frac{\sin i_h}{\cos i_h} \frac{d^2 T}{d\Delta^2} = \frac{\alpha_h^2}{r_h^2} \frac{1}{\cos i_h} \frac{dT}{d\Delta} \frac{d^2 T}{d\Delta^2}. \qquad (12)$$

Assuming that the distance derivatives $dT/d\Delta$ and $d^2T/d\Delta^2$ vary only slightly across the mantle discontinuities, together with $\cos i_h$ which at large distances is always close to 1, one predicts a ratio of amplitudes at constant distance Δ for a source crossing a discontinuity from top to bottom

$$R = \frac{A^{\text{bottom}}}{A^{\text{top}}} = \left[\frac{\rho_h^{\text{top}}}{\rho_h^{\text{bottom}}} \right]^{1/2} \cdot \left[\frac{\alpha_h^{\text{top}}}{\alpha_h^{\text{bottom}}} \right]^2 \qquad (13)$$

equal to 0.86 and 0.88, for the 410- and 660-km discontinuities, respectively, in the *ak135* model. In turn, this predicts an increase in q_{SO} of 0.066 and 0.056 logarithmic units respectively, in general agreement with our results (Fig. 5).

Similarly, at the Mohorovičić discontinuity ($h = 35$ km in *ak135*; D_M on Fig. 5), R is expected to fall to ∼0.61 and the jump in q_{SO} to reach 0.2 logarithmic units, again in good agreement with our results.

(E) At the greatest distances ($\Delta > 85°$) and for all depths, q_{SO} features a regular and strong increase with Δ, on the order of 0.04 logarithmic unit per degree, which compensates for the decrease of the geometrical spreading factor $g(\Delta)$ expressing the divergence of seismic rays bottoming in the deepest layers of the mantle. This feature, which corresponds to a loss of curvature in the travel time $T(\Delta)$, was recognized even in early travel time tables, and is therefore also present in q_{56}, albeit with a greater amplitude of ∼0.055 unit/degree, and in q_{VC} (at 0.065 unit deg^{-1}). Note that this gradient with distance becomes even larger in q_{56} beyond 102°, where however geometrical optics no longer applies to the phase P_{diff}, and which at any rate lies beyond our domain of study.

4.2 Statistics

In Table 1, we examine statistics for comparison of the various corrections $q(\Delta, h)$. For each couple of models q_A and q_B, we define a residual

$$r_{A,B}(\Delta, h) = q_A(\Delta, h) - q_B(\Delta, h) \qquad (14)$$

and list its minimum and maximum values, average $<r>$ and standard deviation σ over the distance–depth domain, the median, 10th- and 90th-percentile values of r, the average $<|r|>$ of its absolute value, and the slope and zero-offset of the best-fitting regression ($q_A = a\, q_B + b$), as well as its relevant correlation coefficient.

We first focus on the comparison between the corrections q_{SO}, developed from our synthetics, and q_{56} mandated by the Prague formula (Kárník *et al.* 1962) and the more recent IASPEI working group (Anonymous 2013). The relevant residual $r_{SO,56}(\Delta, h)$ is contoured on Fig. 6. While the residuals do range from −0.89 to 0.74 units, these extreme values are concentrated at the corners of the (Δ, h) domain; otherwise, the only large, negative r are concentrated at shallow depths, especially for short distances when paths sample primarily the crust, where the model used in our study features the lowest anelastic attenuation (Montagner & Kennett 1996). In the rest of the (Δ, h) plane, the residuals are much smaller, leading to an overall average value of $<r_{SO,56}> = 0.12$ with a standard deviation $\sigma = 0.34$. This general agreement reflects more
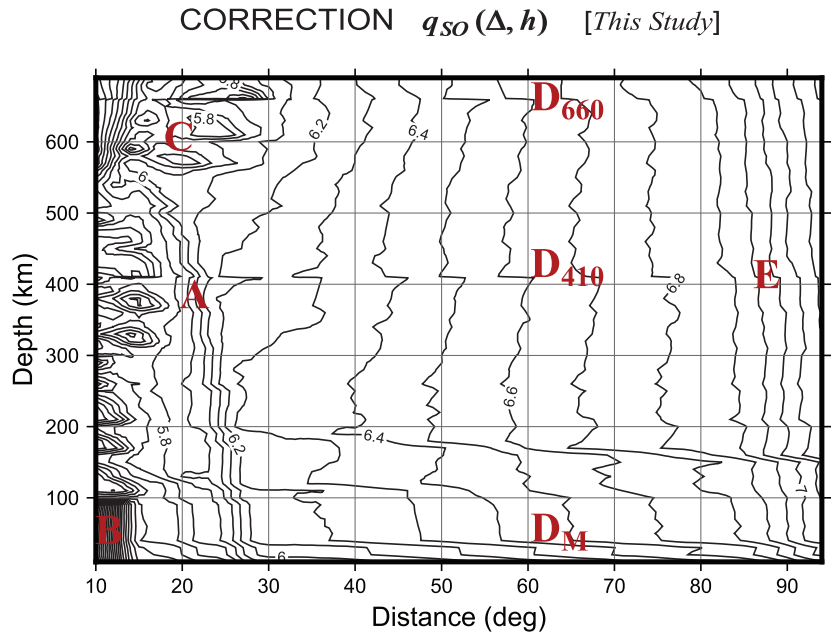
Figure 5. Contoured plot of the correction $q_{SO}(\Delta, h)$ obtained in the present study. Labels refer to features described in text.
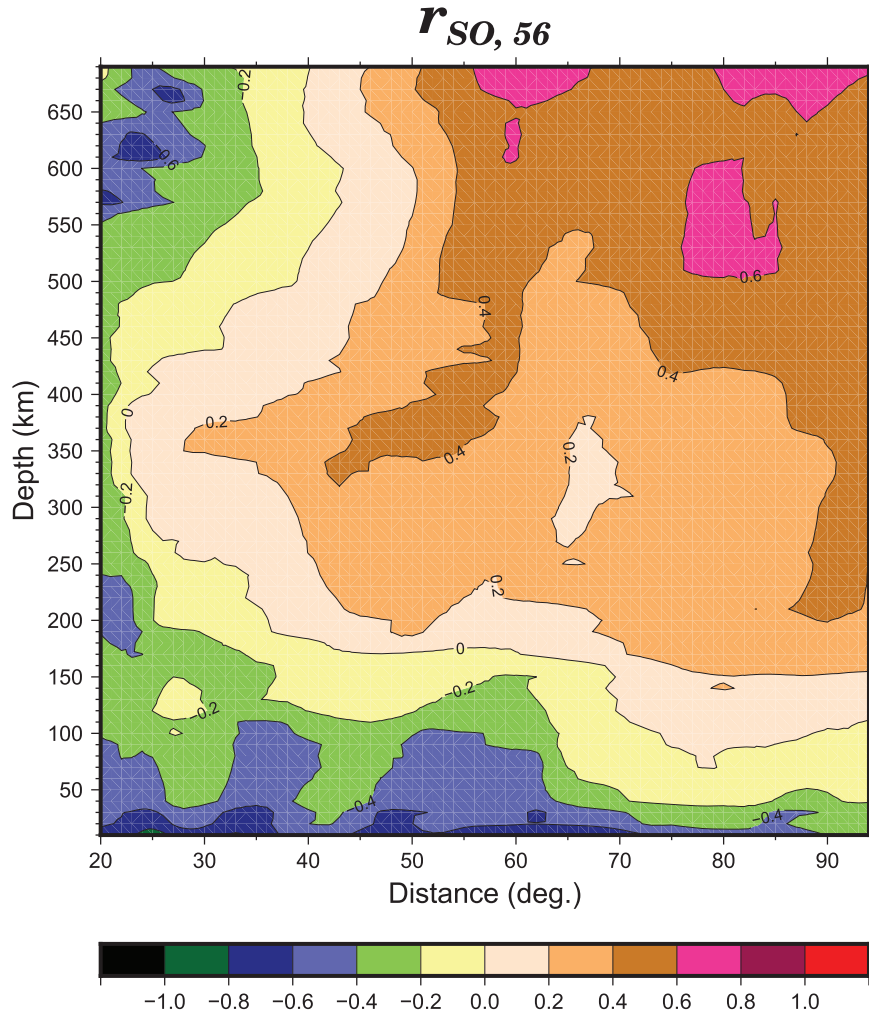

Figure 6. Contoured plot of the residual $r_{SO, 56}$. Note the general increase with distance and depth.

a good average fit than a similarity in pattern, since the correlation coefficient between q_{SO} and q_{56} is mediocre (0.37), suggesting that local fluctuations in the empirical q_{56} are not reflected in the more theoretical q_{SO}.

Remarkably, these conclusions are essentially unchanged when comparing q_{SO} with the original correction q_{45} (Fig. 7a). Expectedly, since the latter is less smooth than q_{56}, the extreme values of $r_{SO, 45}$ (−1.01 and 0.94) are somewhat larger, but the average properties ($< r_{SO, 45} > = 0.08$ and $\sigma = 0.36$) are comparable to the previous case with, however, an even smaller correlation coefficient (0.30); similarly, the 10th- and 90th-percentile values are essentially identical for $r_{SO, 56}$ and $r_{SO, 45}$.

The poorest fit is obtained when comparing q_{SO} with Veith & Clawson's (1972) q_{VC}, the residuals being systematically positive ($< r_{SO, VC} > = 0.47$ or a factor of nearly 3 on ground motion amplitude). However, because q_{VC} is a smoother function than q_{56}, its correlation coefficient with q is slightly higher (0.46). On the opposite, q_{VC} has a significantly better coefficient correlation with q_{56} (0.79), despite its systematic negative bias.

In addition, an interesting comparison is that between the two versions of the founding fathers' correction, Gutenberg's (1945b) original q_{45} and Gutenberg & Richter's (1956) more definitive q_{56} (Fig. 7d). The minimum value of the residual $r_{56, 45}$ (−0.54 at $\Delta = 45°$; $h = 350$ km) reflects a nearly universal local maximum in q_{45} at that distance and for all depths, as opposed to a more local low in q_{56}, which drops below 6.0 in that region, both features remaining unexplained. The maximum value $r_{max} = 0.54$ relates to a pronounced low in q_{45} which drops below 6.2 at ($\Delta = 90°$; $h = 350$ km) in the midst of the regular increase of q with Δ observed in all models at those large distances. Again, the origin of this feature is unexplained. Otherwise, the correlation between the two models is good (0.70), and the average residual and standard deviation are minimal (0.04 ± 0.19 logarithmic units), confirming the 'consanguinity' of the models, q_{56} having been, unavoidably if mysteriously, derived from q_{45}.

Finally, and expectedly, replacing q_{56} with its smoothed version q_{JD} leaves all statistics practically unchanged.

4.3 Spectra

Fig. 8(a) is a contour plot of the spectral amplitude of the correction q, obtained by taking its double Fourier transform into the spatial frequency plane (k_Δ; k_h). The amplitude is concentrated mainly for a combination of $k_\Delta = 0.05$ rad deg^{-1} and $k_h = 0.005$ rad km^{-1} (albeit with a few side lobes), which would correspond to spatial 'wavelengths' of 125° and 1250 km, respectively. Both express the systematic increase of q_{SO} with Δ (at most depths) and with h (at most distances), over ranges comparable to half those wavelengths. The spectrum is richer in distance than in depth wavenumbers.

Figs 8(b)–(d) similarly examine the spectra of other corrections q. While a low-frequency character is preserved in all cases, q_{56} shows a shift of the maximum spectral components to shorter distance wavelengths ($k_\Delta = 0.1$ rad deg^{-1}), which expresses the different pattern in q_{56} for $\Delta < 55°$ (little variation with distance) and $\Delta > 55°$ (more systematic increase with Δ). As expected, the interpolated 'Working Group' correction q_{JD} has a spectrum (not shown) sharing these properties. By contrast, the spectrum of the much more complex $q_{45}(\Delta, h)$ is clearly blue-shifted to higher spatial frequencies, especially along the distance wavenumber, with a maximum around $k_\Delta = 0.35$ rad deg^{-1}, corresponding to a wavelength of 18°. Finally, Veith & Clawson's (1972) correction q_{VC} is

red-shifted with respect to q_{56}, and its spectrum is reminiscent of that of q_{SO}.

The spectral properties of the various corrections $q(\Delta, h)$ are further examined in Appendix A, where advanced metrics are used to quantify the above results.

4.4 Bias from the distribution of stations across the (Δ, h) plane in the original models

To explore this question, we extracted from the NEIC catalogue all 76 067 earthquakes featuring at least one magnitude $M \geq 5$ for the years 1970–2015, for which source characteristics can be assumed to be accurate by modern standards; the hypocentral distribution of such a data set is expected to be reasonably comparable to those which went into the preparation of the corrections q_{45} and q_{56}. We then plot these individual events on Fig. 9(a) as a function of depth and distance to Pasadena. As expected, large sections of the (Δ, h) plane are not covered, which simply expresses the irregular geographical distribution of subduction zones, but also means that B. Gutenberg had to rely exclusively on mailed-in reports for those combinations of Δ and h. We further the experiment in Fig. 9(b), by including distances, color-coded by stations, to Jena, La Paz, Kobe and Adelaide, which, according to Gutenberg (1945b), contributed, after Pasadena, the largest number of measurements of deep shocks into the q_{45} database.

A reassuring aspect of Fig. 9(b) is that it largely fills the vacant parts in Fig. 9(a); but this apparent blessing may hide a component of curse in disguise, as it suggests that certain domains of the (Δ, h) plane are sampled primarily by a single, or a single group of stations, for example, Pasadena (and other Southern California stations) would control the combination ($\Delta \sim 80°$; $h = 500$–650 km), Kobe, and possibly Japanese stations nearby, ($\Delta \sim 70°$; $h = 500$–650km), and Adelaide, and possibly other Australian stations such as Riverview, ($\Delta \sim 40°$; $h = 500$–650 km).

This could bias the computation of $q(\Delta, h)$ in two ways. First, the instruments in use at these stations could be drastically different from that at Pasadena, which means that the dominant period recorded in the P wave, and hence the windows sampled in the frequency domain would have been different. For example, Adelaide operated a single North–South Milne-Shaw instrument with a period of 12 s, while Jena and Kobe operated Wiechert instruments with periods of 8 and 4 s, respectively. La Paz used a bi-filar system with a period of 2.4 s (McComb & West 1931; Parham *et al.* 1988). In order to illustrate this issue, we built seismograms in the same geometry as on Fig. 4, but using the responses of these various instruments; we also included the case of a modern digital broadband system. The resulting logarithmic values L, listed in Table 2, emphasize that using a different instrument could significantly affect the computed magnitudes, by as much as ∼0.3 logarithmic units. Note in particular that even common types of instruments, such as Wiechert mechanical seismometers, could feature widely differing constants (period and damping parameters), displacing the dominant period beyond the presently mandated upper bound 3 s. In this respect, it is highly probable that a large number of measurements used by B. Gutenberg in the building of q_{45} and q_{56} would now be in violation of the modern algorithm (Anonymous 2013). Not surprisingly, the use of a modern broadband instrument, or of a mechanical system operating far below its pendulum period (e.g. Adelaide) minimizes this potential bias.

As a second source of bias, the combination of Δ and h controlled by a single station often (but not always) corresponds to
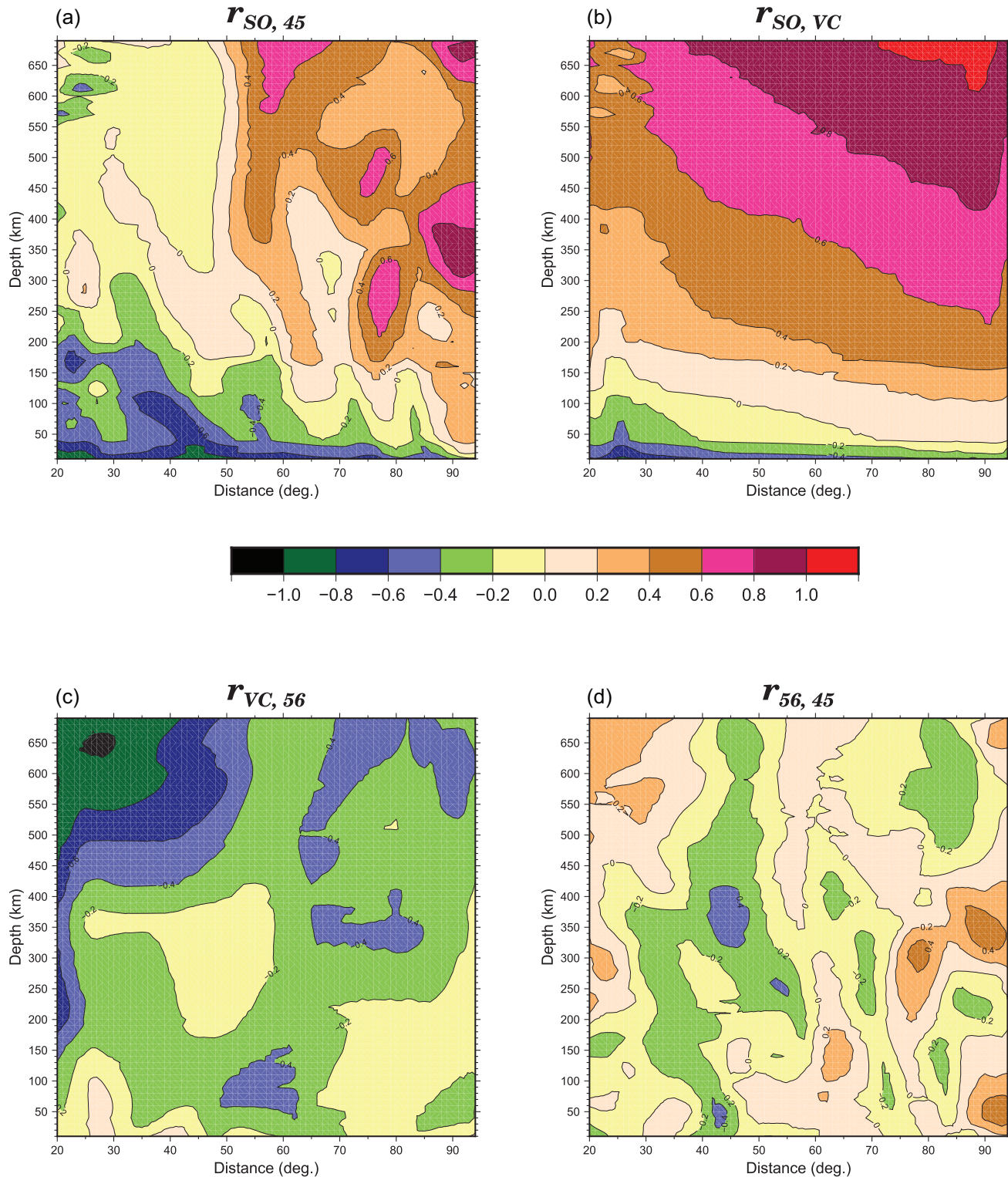
Figure 7. Residuals for other combinations of corrections $q (\Delta, h)$. The same palet is used for all plots in Figs 6 and 7.

a particular geographic epicentral area. For example, deep earthquakes at a distance of ∼80° from Pasadena can sample Fiji, South America and the Sea of Japan and those 40° from Adelaide, Fiji and Java, but events 70° from Kobe are exclusively from Fiji. Since plate dynamics predict that earthquakes at the bottom of subduction zones should have a preferential downdip compressional mechanism (Isacks & Molnar 1971), events from a single region (e.g. Fiji)

will have a consistent radiation pattern coefficient for *P* waves, R^P, to a given station (*e.g.,* Kobe). That could introduce a bias when a single epicenter-station combination controls a domain of distances and depths (in that case, 70° and 500–650 km) in the (Δ, h) plane.

We explore this possibility by examining *P*–wave radiation patterns to the five stations Pasadena, Jena, La Paz, Kobe and Adelaide from all available GlobalCMT solutions (Dziewonski *et al.* 1981;
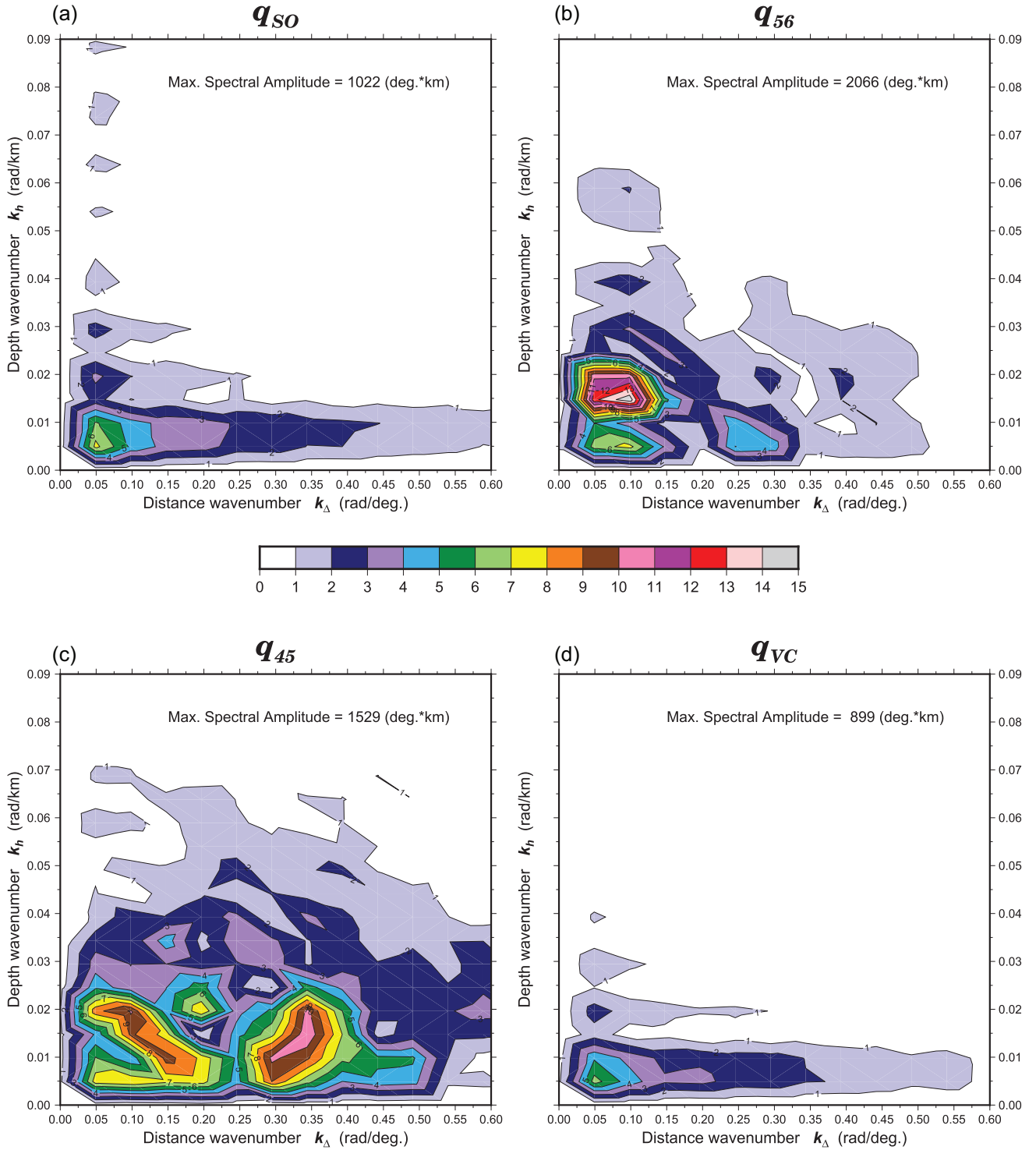
Figure 8. Spectral amplitudes of corrections $q(\Delta, h)$ contoured and colour-coded in the (k_{Δ}, k_h) wavenumber plane. The palet is common to all frames, using a linear scale extending from 0 to 15, the latter corresponding to 2100 deg.km. Except in the case of q_{45} (Frame c), note the preponderance of low-frequency spectral components, and the generally richer spectrum along the k_{Δ} direction.

Ekström *et al.* 2012) with $M_0 > 10^{24}$ dyn∗cm for the years 1977-2018 (a total of 26,571 events). Results, are shown on Fig. 10, color-coded according to the value of $|R^P|$. We recall that its average value over the focal sphere is $2/\sqrt{15} \approx 1/2$. Note that for very shallow sources ($h < 50$ km), radiation patterns trend

systematically from lower values at shorter distances, largely controlled by Kobe and La Paz, in a geometry where rays emerge close to the low-angle plane characteristic of nearby subduction events, to large $|R^P|$ values beyond 70° where the continental stations Pasadena and Jena come into play. Deficient amplitudes may have
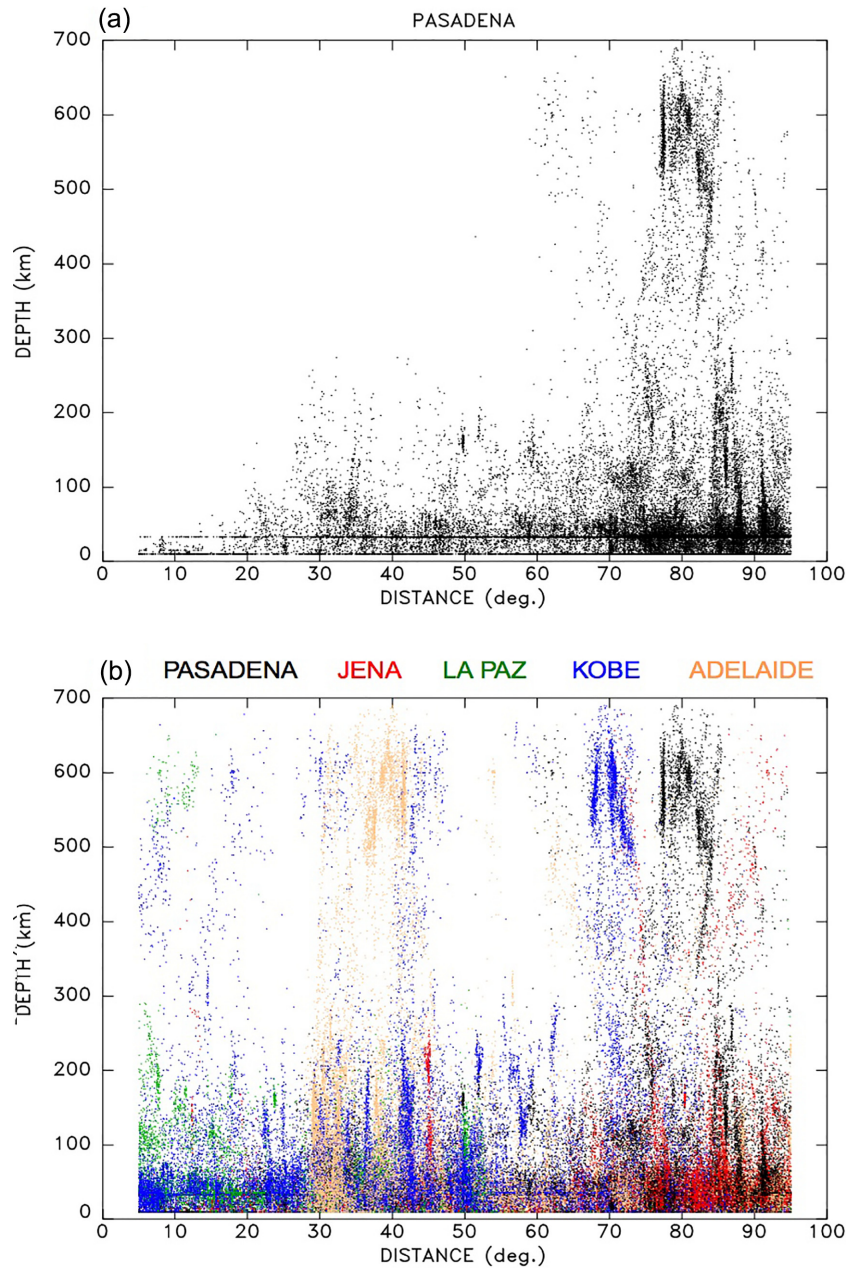
Figure 9. (a) Distribution of recent seismicity (1970–2015; $M \geq 5$) as a function of source depth and distance to Pasadena. Note that large sections of the (Δ, h) plane lack coverage. (b) Same as (a) but including distances to four other stations contributing the bulk of Gutenberg's (1945b) data set for deep earthquakes, colour-coded according to stations. Note that several regions of the (Δ, h) plane are covered principally or exclusively by one of the five stations.

induced the founding fathers to artificially increase q_{56} at shorter distances; this effect could account for a bias of ~0.12 logarithmic units out of the 0.35 observed for $r_{SO, 56}$ across the full distance range (Fig. 6). Rapid variations as a function of distance are also observed at great depths ($h > 500$ km), *e.g.,* in the interval $67° \leq \Delta \leq 75°$, including many large values greater than 0.75 (shown as red dots), as opposed to generally lower values in the 75-85° window. However, a direct correlation with the corrections q_{56} or q_{45} is not present. Without precise information on the events which formed the data sets used in the preparation of those corrections, we can only speculate as to the possibility of any bias introduced by systematic focal geometries in deep portions of the (Δ, h) plane.

5 CONCLUSION AND PERSPECTIVE: A PRELIMINARY TEST OF q_{SO} VERSUS q_{JD}

We have explored the origin of the correction $q(\Delta, h)$ used for the computation of the body-wave magnitude m_b (1), defined on a largely empirical basis by Gutenberg (1945b) as q_{45}, revised as q_{56} by Gutenberg & Richter (1956), and later enshrined into operational practice (Kárník *et al.* 1962; Anonymous 2013). Using a large number of synthetic seismograms computed for a full range of source depths and station distances, but at constant seismic moment, we obtain our own correction $q_{SO}(\Delta, h)$. While it retains some commonality with the original versions of q, especially at low distance and depth wavenumbers, we could not find any explanation for the small-scale variations over the (Δ, h) plane of q_{56}, and

Table 2. Influence of instrumentation on m_b measurements.

	System simulated				S_{max}	T	G	A	L
Instrument	Station	T_p (s)	V	ϵ	(cm[†])	(s)		(μm)	
				Historical instruments					
Benioff SP (Fig.4)	Pasadena		Electromagnetic		5.03	1.53	9120	5.52	0.56
Wiechert	Jena	8	21	3.5	0.38	3.91	509	7.45	0.28
Bi-filar	La Paz	2.4	700	2	0.96	2.52	1506	6.37	0.40
Wiechert	Kobe	3.1	61	4.6	0.64	3.20	67	9.64	0.48
Milne-Shaw	Adelaide	12	150	20	0.24	3.97	150	16.07	0.61
				Modern digital instrument					
STS-2	GSN		Broad-band digital		1.016×10^8	2.80	8.204×10^{10}	12.39	0.65

Note: † Units are digital counts in the case of the digital instrument
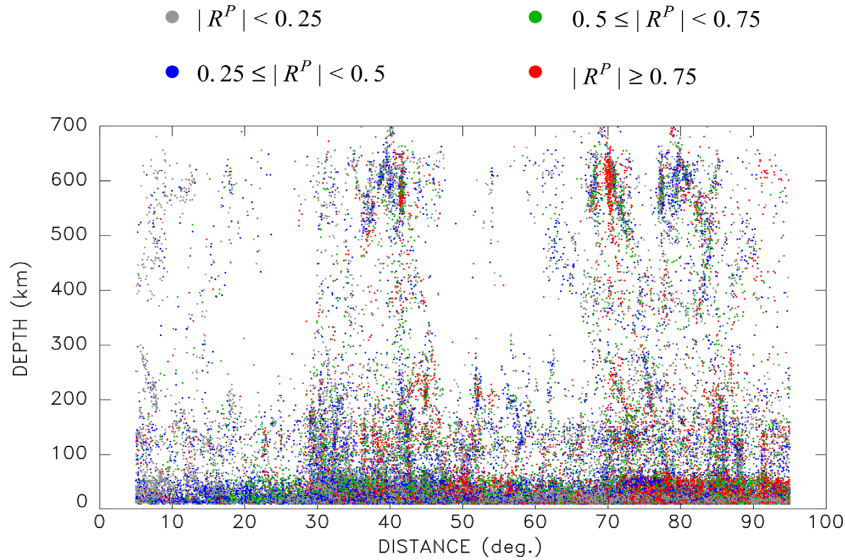

Figure 10. Distribution of GlobalCMT sources ($M_0 \geq 10^{24}$ dyn∗cm) color-coded according to absolute radiation patterns $|R^P|$ at the five stations in Fig. 9, as a function of station distance and source depth. A prominent color in a subsection of the diagram could indicate a systematic bias during an empirical determination of q.

especially of q_{45}. Seventy-five years after the original papers were published, their origin thus remains a mystery. However, we identify some possible sources of systematic bias which may have played a role in the inclusion of fine structure in the corrections q_{45} and q_{56}. Another one, possibly more subtle, but no less systematic, is the expected variation of period with Δ and h, whose effect is analysed in Appendix B.

Having derived a new correction $q_{SO}(\Delta, h)$ more solidly rooted in modern theory than its empirical predecessor q_{56} (and its operational version q_{JD}), the question arises naturally of the effect that its use would have on the routine computation and cataloging of m_b. For this purpose, we ran an exploratory test based on a small data set of 17 large earthquakes, listed in Table 3 in order of increasing depth, from 14 to 687 km. For each of them, we extracted from the ISC Bulletin reported values of amplitude A and period T, and proceeded to recompute values of m_b through eq. (1), using both the correction q_{JD} standardized by the Working Group (Anonymous 2013) and our newly derived q_{SO}. We list in the last column of Table 3 and plot on Fig. 11 the residual $[(m_b)_{SO} - (m_b)_{JD}]$, which is simply $r_{SO, JD}$ (eq. 14), for the appropriate source depth and averaged over the reporting stations. A clear trend is present, which

regresses with a slope of ∼0.1 logarithmic unit per 100 km (red line on Fig. 11). At shorter distances, our data set clearly follows the green curve, which plots, as a function of h, the theoretical average of $r_{SO, JD}$ between $\Delta_{min} = 20°$ and $\Delta_{max} = 94°$:

$$\overline{r_{SO, JD}}(h) = \frac{1}{\Delta_{max} - \Delta_{min}} \cdot \int_{\Delta_{min}}^{\Delta_{max}} r_{SO, JD}(\Delta, h) \cdot d\Delta \quad (15)$$

The agreement simply expresses that the average residual taken over the reporting stations is comparable to the residual averaged mathematically over all distances, or in other words that the distribution of stations over distance is appropriately regular. However, we note that the fit between our data set and the predicted residual (green curve on Fig. 11) deteriorates for $h > 400$ km. To interpret this effect, we plot as the blue dashed line average residuals (15) computed for $\Delta_{min} = 50°$, which is in better agreement with outliers in our data set. The difference between the green and blue curves reflects that $r_{SO, 56}$ has a weak distance gradient for shallow sources, but a much stronger one at greater depths (Fig. 6). We have verified that indeed outlying events such as the 2008 Sea of Okhotsk and 1994 Bolivia and Primorye earthquakes have a dis-

Table 3. Events used in preliminary test.

| Date	Region	Latitude	Longitude	Depth	m_b		
D M (J) Y		(°N)	(°E)	(km)	From q_{JD}	From q_{SO}	Residual
28 OCT (302) 2012	Haida Gwaii	52.79	−132.10	14	6.44	5.82	−0.62
03 MAY (123) 2006	Tonga	−20.19	−174.12	55	7.04	6.85	−0.19
04 OCT (277) 1994	Kuril Islands	43.60	147.63	68	7.23	7.03	−0.20
23 JUN (174) 2014	Aleutian Is.	52.00	178.43	104	6.59	6.51	−0.08
22 JAN (022) 2017	Solomon Is.	−6.03	154.94	150	6.89	6.85	−0.04
29 JUL (211) 2016	Mariana Is.	18.50	145.70	209	6.63	6.82	0.19
08 AUG (220) 2007	Java	−6.03	107.58	305	6.10	6.35	0.25
27 JAN (027) 2006	Banda Sea	−5.61	128.20	397	6.91	7.20	0.29
21 JUL (202) 1994	Primorye	42.34	132.87	460	6.41	6.79	0.38
24 NOV (329) 2008	Sea of Okhotsk	54.20	154.32	492	6.49	6.91	0.42
05 FEB (036) 2005	Mindanao	5.29	123.34	540	6.34	6.62	0.28
19 AUG (231) 2018	South of Fiji	−17.86	−177.85	555	6.92	7.09	0.17
17 JUN (169) 1996	Flores Is.	−7.38	123.02	584	6.39	6.61	0.22
24 MAY (144) 2013	Sea of Okhotsk	54.61	153.77	611	7.34	7.68	0.34
09 JUN (160) 1994	Bolivia	−13.82	−67.25	647	7.04	7.56	0.52
30 MAY (150) 2015	Bonin Islands	27.94	140.56	681	7.04	7.47	0.43
06 SEP (249) 2018	South of Fiji	−18.24	179.86	687	6.50	6.80	0.30
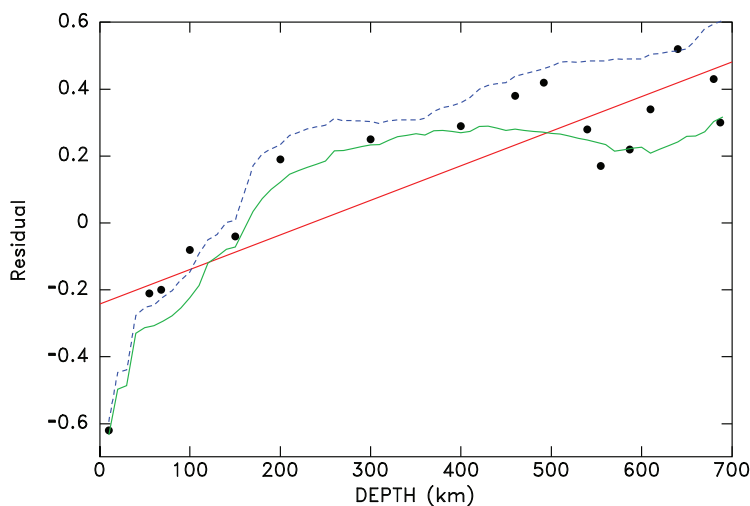
Figure 11. Exploratory experiment comparing magnitudes computed using q_{JD} and q_{SO} from amplitude and period data actually reported to the ISC for 17 large earthquakes. The individual dots are the differences in magnitudes listed in the last column of Table 3. The red line is their linear regression as a function of depth. Also shown are the predicted average residuals from eq. (15) for $\Delta_{min} = 20°$ (solid green curve) and $\Delta_{min} = 50°$ (dashed blue curve).

tribution of amplitude-reporting stations strongly biased towards greater distances, with for example, the Bolivian earthquake having none below 55°. This remark emphasizes the possibility of further and subtle biases in the computation of m_b.

It is clear that this limited experiment constitutes only a partial result, on account on the meager size of the processed data set. However, it would suggest that a systematic bias exists when comparing catalogued m_b values for shallow and deep earthquakes, which may be close to a full logarithmic unit; we recall that such comparisons were the driving force behind the extension of magnitude scales to deep sources by Gutenberg (1945b). The inescapable conclusion would then be the need to revise the entire existing catalogue of published values of m_b. This truly herculean project obviously falls beyond the scope of the present paper.

ACKNOWLEDGEMENTS

REFERENCES

Anderson, D.L., Ben-Menahem, A. & Archambeau, C.B., 1965. Attenuation of seismic energy in the upper mantle, *J. geophys. Res.,* **70**(6), 1441–1448.

Anonymous, 2013. Summary of magnitude working group recommendations on standard procedures for determining earthquake magnitudes from digital data, *Int. Assoc. Seismol. Phys. Earth Inter.,* http://iaspei.org/commissions/commission-on-seismological-observation-and-interpretation/Summary_WG_recommendations_20130327.pdf.

Benioff, H., 1932. A new vertical seismograph, *Bull. seism. Soc. Am.,* **22**(2), 155–169.

Bondár, I., Engdahl, E.R., Villaseñor, A., Harris, J. & Storchak, D., 2015. ISC-GEM: global instrumental Earthquake Catalogue (1900–2009), II. Location and seismicity patterns, *Phys. Earth planet. Inter.,* **239,** 2–13.

Borcherdt, R.D., 1970. Effects of local geology on ground motion near San Francisco Bay, *Bull. seism. Soc. Am.,* **60**(1), 29–61.

Bouchon, M., 1973. Effect of topography on surface motion, *Bull. seism. Soc. Am.,* **63**(2), 615–632.

Burdick, L. & Helmberger, D.V., 1978. The upper mantle *P* velocity structure of the Western United States, *J. geophys. Res.,* **83**(B4), 1699–1712.

Carpenter, E., 1965. Attenuation of teleseismic body waves, *Nature,* **207,** 745–746.

Carpenter, E., 1966. A quantitative evaluation of teleseismic explosion records, *Proc. R. Soc. Lond., A.,* **290**(1422), 396–407.

Chao, B.F., Gross, R.S. & Dong, D.-N., 1995. Changes in global gravitational energy induced by earthquakes, *Geophys. J. Int.,* **122**(3), 784–789.

Choy, G.L. & Boatwright, J.L., 1995. Global patterns of radiated seismic energy and apparent stress, *J. geophys. Res.,* **100**(B9), 18 205–18 228.

Choy, G.L., McGarr, A., Kirby, S.H. & Boatwright, J., 2006. An overview of the global variability in radiated energy and apparent stress, *Am. Geophys. Un. Geophys. Monogr. Ser.,* **170,** 43–57.

Der, Z., McElfresh, T., Wagner, R. & Burnetti, J., 1985. Spectral characteristics of *P* waves from nuclear explosions and yield estimation, *Bull. seism. Soc. Am.,* **75**(2), 379–390.

Dziewonski, A., Chou, T.-A. & Woodhouse, J., 1981. Determination of earthquake source parameters from waveform data for studies of global and regional seismicity, *J. geophys. Res.,* **86**(B4), 2825–2852.

Ebeling, C.W. & Okal, E.A., 2012. An extension of the E/M_0 tsunami earthquake discriminant Θ to regional distances, *Geophys. J. Intl.,* **190**(3), 1640–1656.

Ekström, G., Nettles, M. & Dziewoński, A., 2012. The GlobalCMT project 2004–2010: centroid-moment tensors for 13,017 earthquakes, *Phys. Earth planet. Inter.,* **200,** 1–9.

Evernden, J.F., 1967. Magnitude determination at regional and near-regional distances in the United States, *Bull. seism. Soc. Am.,* **57**(4), 591–639.

Geller, R.J., 1976. Scaling relations for earthquake source parameters and magnitudes, *Bull. seism. Soc. Am.,* **66**(5), 1501–1523.

Gutenberg, B., 1945a. Amplitudes of *P*, *PP*, and *S* and magnitude of shallow earthquakes, *Bull. seism. Soc. Am.,* **35**(2), 57–69.

Gutenberg, B., 1945b. Magnitude determination for deep-focus earthquakes, *Bull. seism. Soc. Am.,* **35**(3), 117–130.

Gutenberg, B., 1957. Effects of ground on earthquake motion, *Bull. seism. Soc. Am.,* **47**(3), 221–250.

Gutenberg, B. & Richter, C., 1936. On seismic waves (Third paper), *Gerlands Beitr. Geophys,* **47,** 73–131.

Gutenberg, B. & Richter, C.F., 1942. Earthquake magnitude, intensity, energy, and acceleration, *Bull. seism. Soc. Am.,* **32**(3), 163–191.

Gutenberg, B. & Richter, C.F., 1954. *Seismicity of the Earth,* 310 pp., Princeton Univ. Press.

Gutenberg, B. & Richter, C.F., 1956. Magnitude and energy of earthquakes, *Anna. Geof.,* **9,** 1–15.

Haskell, N.A., 1962. Crustal reflection of plane *P* and *SV* waves, *J. geophys. Res.,* **67**(12), 4751–4768.

Herrin, E., 1968. Introduction to "1968 seismological tables for *P* phases", *Bull. seism. Soc. Am.,* **58**(4), 1193–1195.

Herrmann, R.B., 2013. Computer programs in seismology: an evolving tool for instruction and research, *Seismol. Res. Lett.,* **84**(6), 1081–1088.

Hudson, J., 1969. A quantitative evaluation of seismic signals at teleseismic distances – I. Radiation from point sources, *Geophys. J. R. astr. Soc.,* **18**(3), 233–249.

Isacks, B. & Molnar, P., 1971. Distribution of stresses in the descending lithosphere from a global survey of focal-mechanism solutions of mantle earthquakes, *Rev. Geophys.,* **9**(1), 103–174.

Johnson, L.R., 1967. Array measurements of *P* velocities in the upper mantle, *J. geophys. Res.,* **72**(24), 6309–6325.

Julian, B.R. & Anderson, D.L., 1968. Travel times, apparent velocities and amplitudes of body waves, *Bull. seism. Soc. Am.,* **58**(1), 339–366.

Kárník, V., Kondorskaya, N., Riznitchenko, J.V., Savarensky, E., Soloviev, S., Shebalin, N., Vaněk, J. & Zátopek, A., 1962. Standardization of the earthquake magnitude scale, *Stud. Geophys. Geod.,* **6**(1), 41–48.

Kennett, B. L.N., Engdahl, E.R. & Buland, R., 1995. Constraints on seismic velocities in the Earth from travel times, *Geophys. J. Intl.,* **122**(1), 108–124.

Knopoff, L. & Gilbert, F., 1959. Radiation from a strike-slip fault, *Bull. seism. Soc. Am.,* **49**(2), 163–178.

Marshall, P., Springer, D. & Rodean, H., 1979. Magnitude corrections for attenuation in the upper mantle, *Geophys. J. R. astr. Soc.,* **57**(3), 609–637.

McComb, H.E. & West, C.J., 1931. List of seismological stations of the world, *Bull. Natl. Res. Council,* 52, 1–119.

Milne, J., 1898. *Seismology,* 1st edn, 146 pp., Trench Trübner.

Montagner, J.-P. & Kennett, B., 1996. How to reconcile body-wave and normal-mode reference Earth models, *Geophys. J. Intl.,* **125**(1), 229–248.

Newman, A.V. & Okal, E.A., 1998. Teleseismic estimates of radiated seismic energy: the E/M_0 discriminant for tsunami earthquakes, *J. geophys. Res.,* **103,** 26 885–26 898.

North, R.G., 1977. Station magnitude bias—its determination, causes, and effects, Tech. rep. 197724, MIT Lincoln Lab, Cambridge, MA.

Okal, E.A., 1992. A student's guide to teleseismic body-wave amplitudes, *Seismol. Res. Lett.,* **63**(2), 169–180.

Okal, E.A., 2019. Energy and magnitude: a historical perspective, *Pure appl. Geophys.,* **176**(9), 3815–3849.

Okal, E.A. & Jo, B.-G., 1990. *Q* measurements for phase *X* overtones, *Pure appl. Geophys.,* **132**(1–2), 331–362.

Parham, R., Greenhalgh, S. & McCue, K., 1988. The South Australian seismic network, *BMR J. Aust. Geol. Geophys.,* **10,** 345–355.

Peacock, S., Douglas, A. & Bowers, D., 2017. Joint maximum-likelihood magnitudes of presumed underground nuclear test explosions, *Geophys. J. Intl.,* **210**(2), 621–644.

Peterson, J. & Hutt, C.R., 2014. World-wide standardized seismograph network: a data users guide, US Geological Survey, Open-File Report, 2014–1218, pp. 82.

Poli, P. & Prieto, G.A., 2016. Global rupture parameters for deep and intermediate-depth earthquakes, *J. geophys. Res.,* **121**(12), 8871–8887.

Richter, C.F., 1935. An instrumental earthquake magnitude scale, *Bull. seism. Soc. Am.,* **25**(1), 1–32.

Richter, C.F., 1958. *Elementaty Seismology,* 768 pp., W.H. Freeman and Company.

Ringdal, F., 1986. Study of magnitudes, seismicity, and earthquake detectability using a global network, *Bull. seism. Soc. Am.,* **76**(6), 1641–1659.

Romanowicz, B. & Mitchell, B., 2015. Deep earth structure: *Q* of the Earth from crust to core, *Treatise on Geophysics,* 789–827.MMMM

Salaree, A., 2019. Theoretical and computational contributions to the modeling of global tsunamis, *PhD dissertation,* 359 pp., Northwestern University.

Saloor, N. & Okal, E.A., 2018. Extension of the energy-to-moment parameter Θ to intermediate and deep earthquakes, *Phys. Earth planet. Inter.,* **274,** 37–48.

Stein, S., Spencer, B.D. & Brooks, E.M., 2015. Metrics for assessing earthquake-hazard map performance, *Bull. seism. Soc. Am.,* **105**(4), 2160–2173.

Teng, T.-L., 1968. Attenuation of body waves and the *Q* structure of the mantle, *J. geophys. Res.,* **73**(6), 2195–2208.

Vallée, M., 2013. Source time function properties indicate a strain drop independent of earthquake depth and magnitude, *Nat. Commun.,* **4,** 6.

Vaněk, J., Zátopek, A., Kárník, V., Kondorskaya, N.V., Riznichenko, Y.V., Savarenskiǐ, E.F., Solov'ev, S.L. & Shebalin, N.V., 1962. Standardizatsya shkaly magnitud, *Izv. Akad. Nauk SSSR, Ser. Geofiz.,* **2,** 153–158 [in Russian; English translation, *Bull. USSR Acad. Sci., Geophys. Ser.*, **2,** 108–111, 1962.].

Veith, K. & Clawson, G., 1972. Magnitude from short-period *P*-wave data, *Bull. seism. Soc. Am.,* **62**(2), 435–452.

Vvedenskaya, A., 1956. Opredelenie poleĭ smeshcheniĭ pri zem-
letryaseniyakh s pomoshch'yu teorii dislokatsii, *Akademia Nauk SSSR,
Seria Geofizicheskaya,* **6,** 277–284 [in Russian].

Wessel, P. & Smith, W. H.F., 1991. Free software helps map and display data,
EOS, Trans. Am. Geophys. Un., **72**(41), 441 and 445–446.

Zöppritz, K., Geiger, L. & Gutenberg, B., 1912. Über Erdbebenwellen. V,
Nachr. k. Gess. d. Wiss. z.Göttingen, math.-phys. Kl., pp. 121–206.

APPENDIX A: ADVANCED METRICS USING SPATIAL FILTERING

In this section, we characterize quantitatively the correlation between the various corrections $q(\Delta, h)$ by considering increasingly smoothed variations of these functions. Specifically, each frame n of Fig. A1 shows the correction $q_{SO}^{(n)}$ resulting from applying a low-pass 2-D filter with cut-off values $k_{\Delta}^{(n)}$ and $k_h^{(n)}$ listed in Table A1, and corresponding to filtering wavelengths $\Lambda^{(n)}$ equivalent to n sampling points in distance and depth, respectively.

At each step of smoothing, indexed n, we define a metric characterizing the fit between the filtered versions of two corrections

$$M_{A, B}^{(n)} = \frac{\sum_{i, j} \left(q_A^{(n)}(\Delta_i, h_j) - q_B^{(n)}(\Delta_i, h_j) \right)^2}{\left[\left(\sum_{i, j} [q_A^{(n)}(\Delta_i, h_j)]^2 \right) \cdot \left(\sum_{i, j} [q_B^{(n)}(\Delta_i, h_j)]^2 \right) \right]^{1/2}}$$

(A1)

This formula is adapted from Stein *et al.* (2015) and Salaree (2019), who applied this concept to other 2-D problems in Geophysics. A good fit between the compared data sets is expressed by a low value of the metric M.

We examine here the variation with n of metrics computed between our corrections q_{SO} on the one hand, and the corrections q_{56}, q_{45} or q_{VC} on the other, with $n = 0$ corresponding to the raw unfiltered data sets. In all cases, the average values $< q >$ have been removed before computing the metrics M through (A1). Fig. A2 shows that the metrics generally decrease with increasing n, and that their values stabilize for $n \geq 4$ and are then comparable for all three couples of corrections considered. The asymptotic value for large n, $M_{SO, 56}^{(n)} \approx 0.12$, expresses the systematic linear trend (with Δ and h) controlling q_{SO}, but less prominent, and shifted to slightly higher values of k in the empirical q_{56} (see the spectra on Figs 8a and b). As n is reduced, the irregular components in q_{56} become more important and dominate its pattern at the lowest values $n = 0$ and $n = 2$, leading to enhanced values of M. The situation is essentially unchanged in the case of $M_{SO, 45}^{(n)}$, and interestingly of $M_{SO, VC}^{(n)}$, although the low-n values are more contained for the latter, because of the generally smoother nature of q_{VC}. Finally, Fig. A2 also compares the two original versions, q_{45} and q_{56}; while their profile is similar, the metrics $M_{56, 45}^{(n)}$ are significantly reduced, their asymptotic values ($\sim$0.015) by as much as one order of magnitude, confirming quantitatively that the difference between those two models is mostly contained in t

heir high-frequency spectrum, with their low-frequency components being comparable.
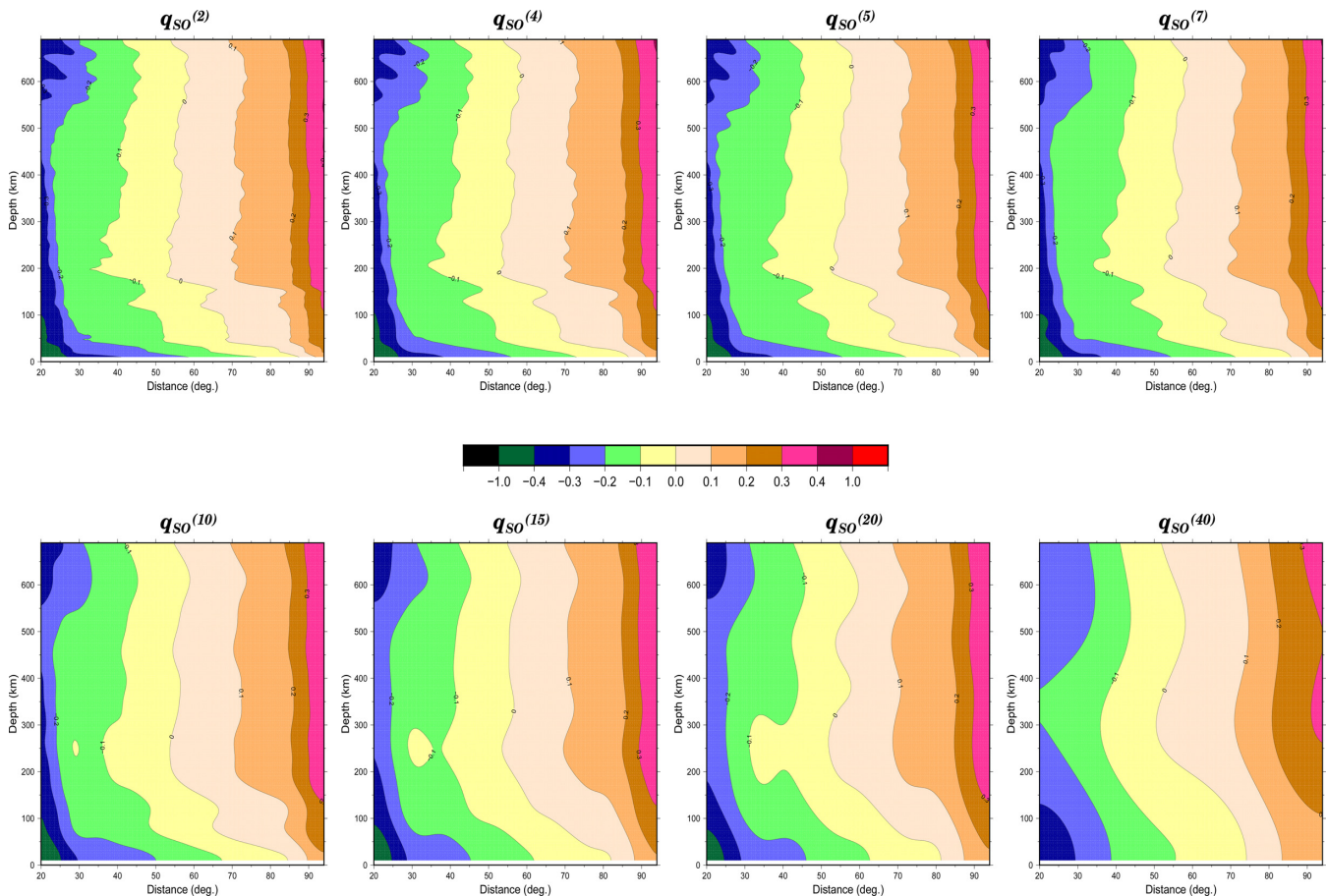

Figure A1. Smoothed versions $q_{SO}^{(n)}(\Delta, h)$ obtained by low-pass filtering the correction q_{SO} at increasingly low maximum wavenumbers, listed in Table A1.
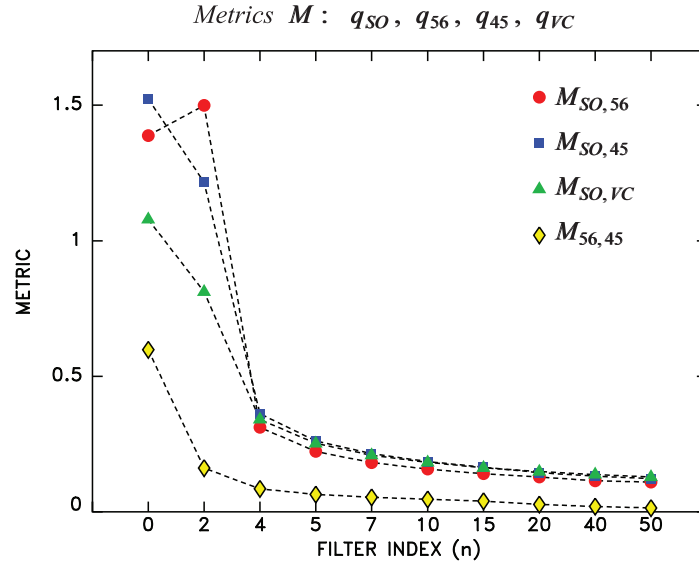
Metrics M : q_{SO} , q_{56} , q_{45} , q_{VC}

Figure A2. Comparison metrics M (eq. A1) for relevant couples of corrections, as a function of the smoothing index n. Note the rapid convergence for $n \geq 4$.

Table A1. Parameters of the smoothing filters used in Fig. A1.

Index n	$k_\Delta^{(n)}$ (rad deg^{-1})	$k_h^{(n)}$ (rad km^{-1})	$\Lambda_\Delta^{(n)}$ (deg)	$\Lambda_h^{(n)}$ (km)
2	3.14	0.314	2	20
4	1.57	0.157	4	40
5	1.26	0.126	5	50
7	0.90	0.009	7	70
10	0.628	0.0628	10	100
15	0.419	0.0419	15	150
20	0.314	0.0314	20	200
40	0.157	0.0157	40	400
50	0.126	0.0126	50	500

This experiment serves to verify quantitatively that some longer-wavelength features of the original corrections q_{45} and q_{56} (in lay terms, their coarser properties) are also expressed in q_{SO} derived from our synthetics, but that any feature of the original corrections with $n \leq 4$ (i.e. on a scale of less than 40 km in depth of 4° in distances) remains unexplained.

APPENDIX B: THE SYSTEMATIC VARIATION OF PERIOD T ACROSS THE (Δ, h) PLANE

We examine here another source of possible bias in m$_b$, namely the systematic variation of the dominant period T across the (Δ, h) plane. Fig. B1 contours the period T resulting from the processing of our synthetics, averaged over all focal geometries, as a function of Δ and h. In simple terms, we find that it increases from ~0.9 s at short distances and for deep events to ~1.8 s at the largest distances and for shallow sources. This is easily explained as a result of the preferential anelastic attenuation of high frequencies, which is more efficient over those paths which are long and/or intensely sample the asthenosphere.

In principle, in order to recover a true ground motion A, the algorithm described on Fig. 4 requires the use of the exact gain G at the relevant period T (Anonymous 2013); in the case of the Benioff

short-period instrument used in our synthetics, the difference in gain between 0.9 and 1.8 s is a factor of 4.5 (or 0.65 logarithmic units). If, for a number of reasons, one uses a constant gain, the instrument response would be underestimated for short distances (and/or deep sources) relative to longer paths (and/or shallow sources), and in turn the ground motions would be overestimated at short distances and underestimated for long paths. When attempting to match measurements made for the same earthquake at various distances, one would then force an artificial, additional increase in q (Δ) (at fixed h) from short to long distances. For example, in the case of shallow sources and as previously noted, $r_{SO, 56}$ increases by about 0.35 unit from -0.7 to -0.35 between 20° and 90° (Fig. 7), while the dominant period T increases from 1.4 to 1.8 s (Fig. B1).

Clearly, it would have been extremely challenging (if not straight impossible) to manually detect such a difference in T, which would amount to 0.2 mm for half-period oscillations on the paper records read by B. Gutenberg, with a typical time scale of 6 cm mn^{-1}. Yet, the difference in gain at such periods represents a factor of 1.8 (or 0.26 logarithmic units), which when combined with the probable radiation pattern bias of 0.12 units mentioned in Section 4.4, could explain the full increase of ~0.35 units in $r_{SO, 56}$. We stress that this interpretation is based of the assumption that B. Gutenberg was using the short-period Benioff instrument, which is supported by a detailed reading of Gutenberg (1945b), even though that use was most probably not exclusive. On the other hand, the variation in dominant period has a negligible effect when using mechanical instruments such as the Wiechert or Milne-Shaw seismometers, since they have an essentially flat response at periods much shorter than that of their pendulum.

This situation could then create a bias between stations operating mechanical *vs.* electromagnetic instruments, that the founding fathers could have sought to compensate with station corrections when such records involved similar distances. However, this effect may have been incorporated directly into q for those combinations of (Δ, h) controlled by single stations operating different instruments or perhaps simply using different operational procedures, that is adjusting or not the gain to the precise period retained at maximum amplitude.
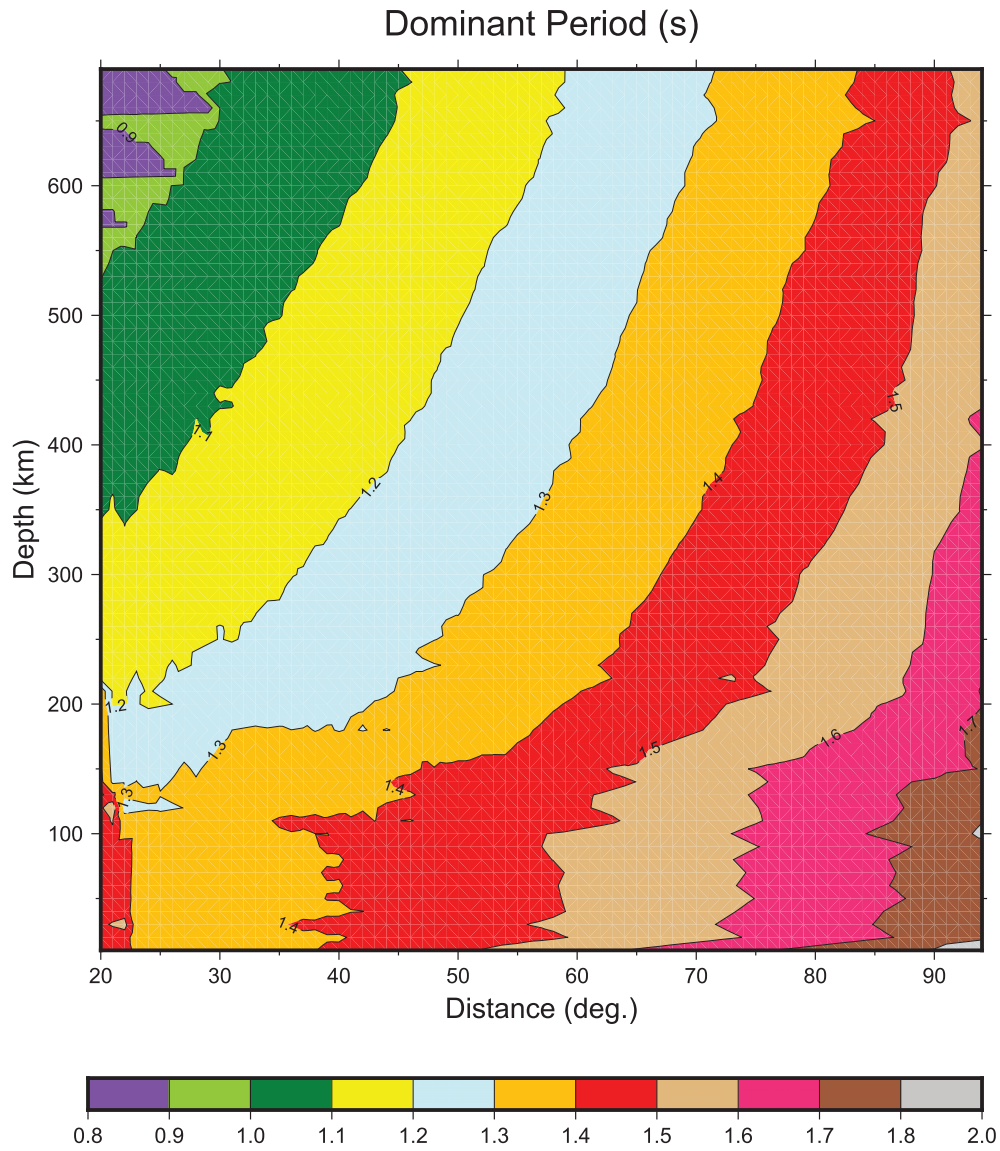
Figure B1. Dominant period T (averaged over all focal geometries) extracted from our synthetic seismograms by the algorithm of Fig. 4, contoured as a function of distance and depth. Note systematic increase with Δ, and decrease with h.